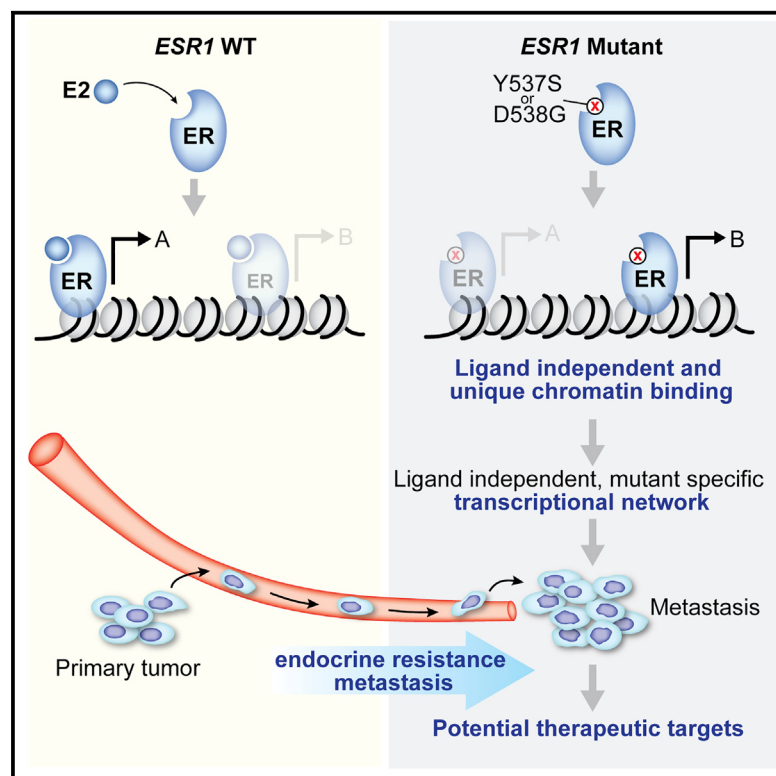


Cancer Cell

Allele-Specific Chromatin Recruitment and Therapeutic Vulnerabilities of ESR1 Activating Mutations

Graphical Abstract



Authors

Rinath Jeselsohn, Johann S. Bergholz,
Matthew Pun, ..., Eric P. Winer,
Jean Zhao, Myles Brown

Correspondence

myles_brown@dfci.harvard.edu

In Brief

Jeselsohn et al. show that estrogen receptor α (ER) mutations found in endocrine treatment-resistant metastatic breast cancers confer not only ligand-independent ER functions, but also allele-specific neomorphic properties. Importantly, the authors identify potential approaches for treating these breast cancers.

Highlights

- The mutant ER cistromes are different from the E2-stimulated WT ER cistrome
- The ER mutant-selective cistromes drive endocrine resistance and metastases
- The ER Y537S and D538G mutants have distinct cistromes and transcriptomes
- THZ1 blocks mutant ER phosphorylation at S118 and inhibits mutant ER cell growth



Allele-Specific Chromatin Recruitment and Therapeutic Vulnerabilities of ESR1 Activating Mutations

Rinath Jeselsohn,^{1,2,3} Johann S. Bergholz,^{4,5} Matthew Pun,^{1,2} MacIntosh Cornwell,^{1,2} Weihan Liu,^{1,2} Agostina Nardone,^{1,2} Tengfei Xiao,^{1,2} Wei Li,^{1,6} Xintao Qiu,¹ Gilles Buchwalter,^{1,2} Ariel Feiglin,⁷ Kayley Abell-Hart,^{4,5} Teng Fei,^{1,2} Prakash Rao,¹ Henry Long,¹ Nicholas Kwiatkowski,^{4,5} Tinghu Zhang,^{4,5} Nathanael Gray,^{4,5} Diane Melchers,⁸ Rene Houtman,⁸ X. Shirley Liu,^{1,6} Ofir Cohen,^{2,9} Nikhil Wagle,^{2,3,9} Eric P. Winer,^{2,3} Jean Zhao,^{4,5} and Myles Brown^{1,2,3,10,*}

¹Center for Functional Cancer Epigenetics, Dana Farber Cancer Institute, Boston, MA 02210, USA

²Department of Medical Oncology, Dana Farber Cancer Institute, Boston, MA 02210, USA

³Department of Medicine, Brigham and Women's Hospital and Harvard Medical School, Boston, MA 02210, USA

⁴Department of Cancer Biology, Dana Farber Cancer Institute, Boston, MA 02215, USA

⁵Department of Biological Chemistry and Molecular Pharmacology, Harvard Medical School, Boston, MA 02215, USA

⁶Department of Biostatistics and Computational Biology, Dana Farber Cancer Institute and Harvard School of Public Health, Boston, MA 02215, USA

⁷Department of Biomedical Informatics, Harvard Medical School, Boston, MA 02215, USA

⁸PamGene International BV, Hertogenbosch 5211, the Netherlands

⁹Broad Institute of MIT and Harvard, Cambridge, MA 02142, USA

¹⁰Lead Contact

*Correspondence: myles_brown@dfci.harvard.edu

<https://doi.org/10.1016/j.ccel.2018.01.004>

SUMMARY

Estrogen receptor α (ER) ligand-binding domain (LBD) mutations are found in a substantial number of endocrine treatment-resistant metastatic ER-positive (ER^+) breast cancers. We investigated the chromatin recruitment, transcriptional network, and genetic vulnerabilities in breast cancer models harboring the clinically relevant ER mutations. These mutants exhibit both ligand-independent functions that mimic estradiol-bound wild-type ER as well as allele-specific neomorphic properties that promote a pro-metastatic phenotype. Analysis of the genome-wide ER binding sites identified mutant ER unique recruitment mediating the allele-specific transcriptional program. Genetic screens identified genes that are essential for the ligand-independent growth driven by the mutants. These studies provide insights into the mechanism of endocrine therapy resistance engendered by ER mutations and potential therapeutic targets.

INTRODUCTION

Estrogen receptor α (ER) plays a key role in normal breast development and breast cancer. Inhibition of ER function by reducing estrogen (E2) levels or by directly antagonizing E2 stimulation of ER is the mainstay treatment for ER^+ breast cancer. These treatments reduce the risk of recurrence when given in the adjuvant setting, and improve outcomes in metastatic disease; however,

resistance to endocrine treatments remains a major clinical problem (Early Breast Cancer Trialists' Collaborative Group et al., 2012).

A number of studies reported recurrent mutations in *ESR1*, the gene encoding ER, in at least 20% of metastatic endocrine-resistant ER^+ breast cancers that are very rarely found in primary tumors (Jeselsohn et al., 2014; Merenbakh-Lamin et al., 2013; Robinson et al., 2013; Toy et al., 2013). The majority of the

Significance

Metastatic ER^+ breast cancer is the leading cause of breast cancer mortality in the developed world. Mutations in the ER LBD confer endocrine therapy resistance and poor outcomes in patients with metastatic disease. Prior studies have shown that these mutations engender constitutive ER activity to promote estrogen-independent growth. Here we show that these mutations also have allele-specific neomorphic properties that, in addition to supporting estrogen-independent growth, promote a metastatic phenotype. Using genetic screens we have identified vulnerabilities in breast cancer cells expressing the ER mutants and wild-type ER. We used these results to develop a therapeutic combination to overcome ER mutant-driven endocrine therapy resistance.



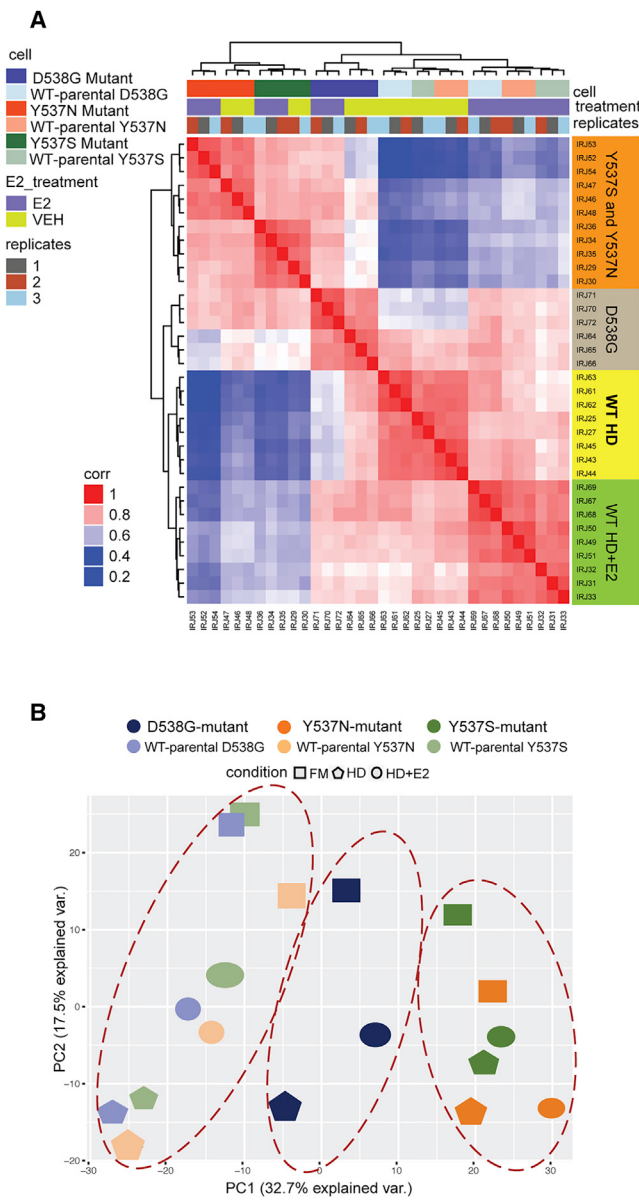


Figure 1. Global Transcriptomic Analysis of the ER Mutant Cell Lines

(A) Pairwise Spearman correlation of RNA-seq between the WT ER parental and mutant cell lines in hormone-depleted (HD) conditions with vehicle (VEH) treatment and HD conditions with estradiol (E2) treatment. Hierarchical clustering shows the relatedness of each sample.

(B) Principal-component analysis of the transcriptomes of WT ER parental cell lines and mutant cell lines in full medium (FM), HD, and HD + E2 conditions. See also Figure S1 and Tables S1 and S2.

recurrent *ESR1* mutations were found to cluster in the ER ligand-binding domain (LBD). Cell line studies showed that the LBD mutations stimulate constitutive activity in the absence of E2, and decreased sensitivity to ER antagonists such as tamoxifen (TAM) and fulvestrant (FUL), indicating that these are gain-of-function mutations and drivers of endocrine resistance (Harrod et al., 2016; Jeselson et al., 2014; Toy et al., 2017).

The two most commonly mutated amino acids are Y537 and D538, which are both within the C-terminal helix of the ER

LBD, helix 12 (H12). Several mutant alleles of Y537 including Y537S, Y537N, and Y537C have been found in endocrine-resistant breast cancers, while only the D538G mutation appears to be a common resistance allele. H12 is a key structural component of the activating function-2 domain of ER that dictates the agonist or antagonist state of the receptor. E2 binding to the LBD leads to stabilization of H12 in an active conformation, enabling the binding of co-activators, such as NCOA3, and results in activation of the receptor. Biophysical studies showed that the Y537S mutation and, to a lesser degree the D538G mutation, stabilize H12 in the agonist conformation, similar to wild-type (WT) ER bound to E2 (Nettles et al., 2008; Fanning et al., 2016). In addition, affinity studies and the crystal structure of the mutant LBD indicate that these mutants have decreased affinity for TAM and E2, and confer an altered conformation facilitating resistance to antagonism. Finally, NCOA3 binding to mutant ER compared with WT ER under ligand-independent conditions, or in the presence of TAM, is enhanced (Fanning et al., 2016; Toy et al., 2013). These findings provide a mechanistic explanation for the ER mutant ligand-independent constitutive-activity and relative resistance to ER antagonists.

The low frequency of the *ESR1* LBD mutations in primary treatment-naïve tumors, the correlation between tumor progression and mutation frequency, and the variable allele frequencies support the clonal selection of these mutations under the selective pressure of endocrine treatment. In addition, we showed that the D538G mutation induces an increased migratory capacity in MCF7 cell models in 2D cell culture (Merenbakh-Lamin et al., 2013). Moreover, the *ESR1* LBD mutations are prognostic of poor outcomes in patients with metastatic disease (Chandarlapaty et al., 2016; Spoerke et al., 2016). These findings imply that, in addition to stimulating E2-independent growth, the *ESR1* LBD mutations may also promote a more aggressive phenotype. This led us to hypothesize that the functional consequences of ER LBD mutations are not restricted to their constitutive activity, but, in addition, lead to changes in the ER transcriptional network that mediate cancer progression. In this study we tested this hypothesis and searched for potential therapeutic targets to overcome the drug resistance and poor outcomes associated with these mutations.

RESULTS

The Mutant ER Transcriptome

To study the global transcriptional changes induced by the ER LBD mutations, we performed RNA sequencing (RNA-seq) of doxycycline (DOX)-inducible mutant ER-expressing cell lines and parental WT ER-expressing cells, in full medium (FM), hormone-depleted (HD) conditions, and HD after stimulation with 1 nM E2 (HD + E2) (Figure 1). These cells expressed the hemagglutinin (HA)-tagged ER LBD mutants and included three of the most common clinical mutations (Y537S, Y537N, and D538G) (Figure S1A). The protein expression of mutant ER was well controlled in these cells, and the combined relative expression of WT and mutant ER protein after DOX induction was comparable with WT ER in the parental cells prior to DOX induction (Table S1). Pairwise correlation analysis of the RNA-seq in HD and HD + E2 clustered the Y537N and Y537S mutant cells in HD and HD + E2 conditions distinctly from the D538G mutant cells and the WT

ER cells. Although the D538G mutant cells clustered with the WT ER cells, they formed a distinct subset. In addition, these data showed that all the WT ER cells clustered together, but were clearly separated by the treatment conditions (HD versus HD + E2). In contrast, the mutant cells in HD and HD + E2 clustered together and the first subclustering was dictated by the specific mutation (Y537S versus Y537N) and not by the medium conditions (Figure 1A). When applying a principal-component analysis to all the samples, principal component 1 (PC1) correlated with the ER mutational status, segregating the WT, the D538G mutant, and the Y537S or Y537N mutant cells; again indicating that the D538G mutation is distinct from the mutations at residue Y537. The medium conditions resolved along PC2 and distinctly clustered the WT cells in FM, HD, and HD + E2 conditions. In the mutant-expressing cells, the HD and HD + E2 conditions aggregated together and segregated away from the FM conditions, supporting the constitutive transcriptional activity of the mutants in the absence of E2 and the difference between FM conditions versus white medium + E2 (Figure 1B). In line with the transcriptional data and prior studies, cell growth in HD and HD + E2 conditions showed that mutant-expressing cells had a growth advantage in HD conditions compared with WT ER-expressing cells. In addition, while WT ER cells displayed marked growth inhibition in HD compared with HD + E2, ER mutant cell growth in HD was only mildly decreased compared with HD + E2 (Figure S1B). We next examined the efficacy of the ER antagonists TAM and FUL in inhibiting mutant ER cell proliferation. While the TAM half maximal inhibitory concentration (IC_{50}) was significantly higher in the MCF7 and T47D cells expressing the Y537S mutant compared with the WT cells, the TAM IC_{50} for D538G ER mutant cells was in the same range as the WT ER cells. Both the Y537S and D538G mutants displayed relative resistance to FUL compared with WT ER cells; however, the resistance was more significant for Y537S compared with D538G. Likewise, the Y537S ER mutant T47D cells had a 31-fold increase in the FUL IC_{50} compared with WT ER T47D cells (Figure S1C; Table S2). These results confirm the relative resistance of the ER LBD mutants to ER antagonists, and also indicate that the Y537S and D538G mutants may be different with respect to response to TAM and FUL.

To further delineate the transcriptional changes induced by the ER-LBD mutations, we performed differential gene expression analyses (Figures S1D and S1E). First, focusing on the WT-expressing cells, comparison of the WT cells (D538G and Y537S DOX-inducible parental cells without DOX treatment) in the absence of E2 (HD) versus E2-stimulated conditions (HD + E2) identified 689 and 814 E2 regulated genes for the D538G and Y537S parental WT ER cell line models, respectively (log₂ fold change [FC] > 0.5, false discovery rate [FDR] < 0.01). As expected, the majority of the E2-regulated genes in the two WT ER cell lines (parental to the D538G and Y537S mutants) overlapped, and among these genes were known ER transcriptional target genes, such as *PGR*, *TFI1*, *GREB1*, *CA12*, *XBP1*, and *MYC* (Figure S1Ea). We next identified the genes that were induced by the ER LBD mutants in HD conditions. We found 308 and 954 genes induced by D538G and Y537S mutants, respectively. Comparison of the genes induced by the mutants in the absence of E2 with the E2-induced genes in WT ER cells revealed that only 33% of the D538G-induced genes and 18%

of the Y537S-induced genes overlapped with genes induced by E2 in WT ER cells (Figure S1Eb). Thus, the majority of the genes induced by the ER mutants in E2-deprived conditions was unique and did not overlap with the WT ER E2-regulated genes. In addition, when we examined the E2-regulated genes in the ER mutant cells, only 12 genes were upregulated by E2 in the Y537S mutant cells, whereas, in the D538G mutant cells, 416 genes were E2 upregulated, and 64% of these genes overlapped with the WT ER E2-regulated genes (Figure S1Ec). Comparison of the D538G- to the Y537S-induced genes showed that 80% of the D538G-induced genes overlapped with the Y537S. In contrast, 74% of the Y537S-induced genes were unique to the Y537S mutation (Figure S1Ed). Taken together, these results support the E2-independent transcriptional activity of the Y537S and D538G mutants, and indicate that these mutations, particularly Y537S, promote the transcription of a unique set of genes that are not induced by E2 stimulation of WT ER. Notably, these results show that the Y537S and D538G mutations induce distinct transcriptional programs, with the D538G mutation driving a transcriptional profile that is more similar to the WT ER E2-dependent transcription compared with the Y537S mutation. Like Y537S, the Y537N allele induced a high number of genes that were not induced by WT ER stimulated by E2 (Figures S1F and S1G).

To address the relevance of these model cell line findings, we evaluated the transcriptome of 109 metastatic tumors from an ongoing study of ER⁺ metastatic breast cancer at the Dana-Farber Cancer Institute. In this study, metastatic tissue biopsies are obtained from patients with ER⁺ disease for genomic and molecular analysis. Global analysis of the RNA-seq data revealed two large clusters of tumors that segregated primarily by the site of metastasis (mets) (Figure 2A). The first cluster of tumors consisted of 42 biopsies exclusively obtained from liver mets and the second cluster included tumor samples from a number of organ sites primarily consisting of tumors from breast, skin, and lung. Hierarchical clustering and principal-component analysis after exclusion of 2,864 genes upregulated in normal liver and skin tissues compared with breast tissue determined by the RNA-seq analysis of healthy liver, skin, and breast tissues from women obtained from the Genotype-Tissue Expression (GTEx) dataset (GTEx Consortium, 2013) (90 breast, 41 liver, and 217 skin samples, log₂ FC > 2 and adjusted p value < 0.001), resulted in the merging of the two clusters (Figures S2A and S2B). This supports the conclusion that these two clusters are driven primarily by gene expression of the normal tissue from the site of the metastatic lesion. We therefore analyzed these two clusters separately for the ensuing analyses. Cluster A was composed of 35 WT ER tumors, 5 ER D538G mutant tumors, 1 ER Y537N mutant tumor, and 1 ER E380Q mutant tumor. Consistent with our previous study, mets harboring the D538G were enriched in the liver mets compared with other metastatic sites (Merenbakh-Lamin et al., 2013). In a supervised analysis of this cluster, we detected a transcriptional profile upregulated in tumors harboring the D538G mutations. Furthermore, gene set enrichment analysis (GSEA) showed that the gene sets of the 100 or 50 top-ranked genes upregulated after induction of the D538G mutation in the MCF7 cell line were enriched in the D538G metastatic tumors compared with the WT ER metastatic tumors in this cluster (normalized

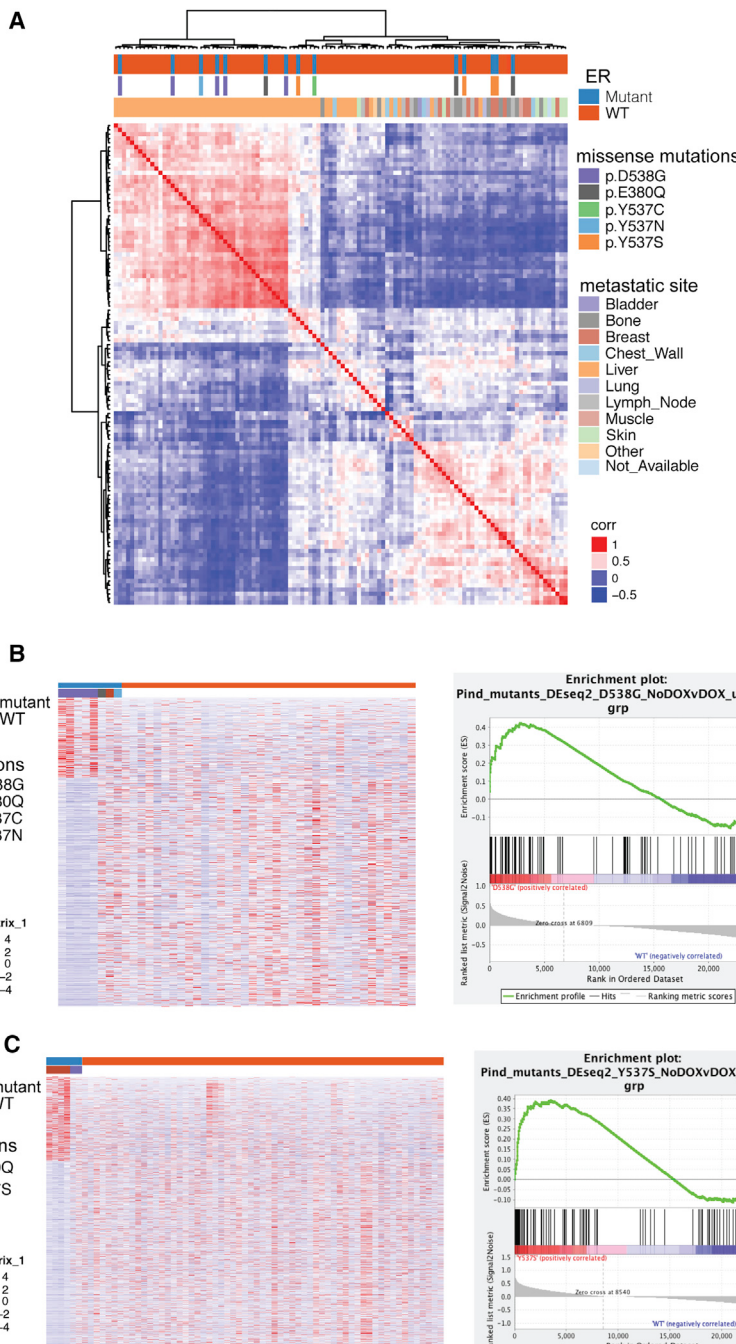


Figure 2. Transcriptomic Analysis of Metastatic Tumors Harboring the *ESR1* LBD Mutations

(A) Pairwise Spearman correlation of RNA-seq between ER⁺ metastatic tumors.

(B) Heatmap of the top 1,000 genes differentially expressed between D538G mutant and WT ER metastatic samples and gene set enrichment (GSEA) plot of the top-ranked 100 genes upregulated with the induction of the D538G mutation in MCF7 cells testing for enrichment in the D538G metastatic tumor samples compared with the WT ER metastatic samples within cluster (A).

(C). Heatmap of the top 1,000 genes differentially expressed between Y537S mutant and WT ER metastatic samples and gene set enrichment plot testing the enrichment of the top-ranked 100 genes upregulated with the induction of the Y537S mutation in MCF7 cells in the Y537S mutant metastatic tumor samples compared with the WT ER metastatic samples within cluster (B).

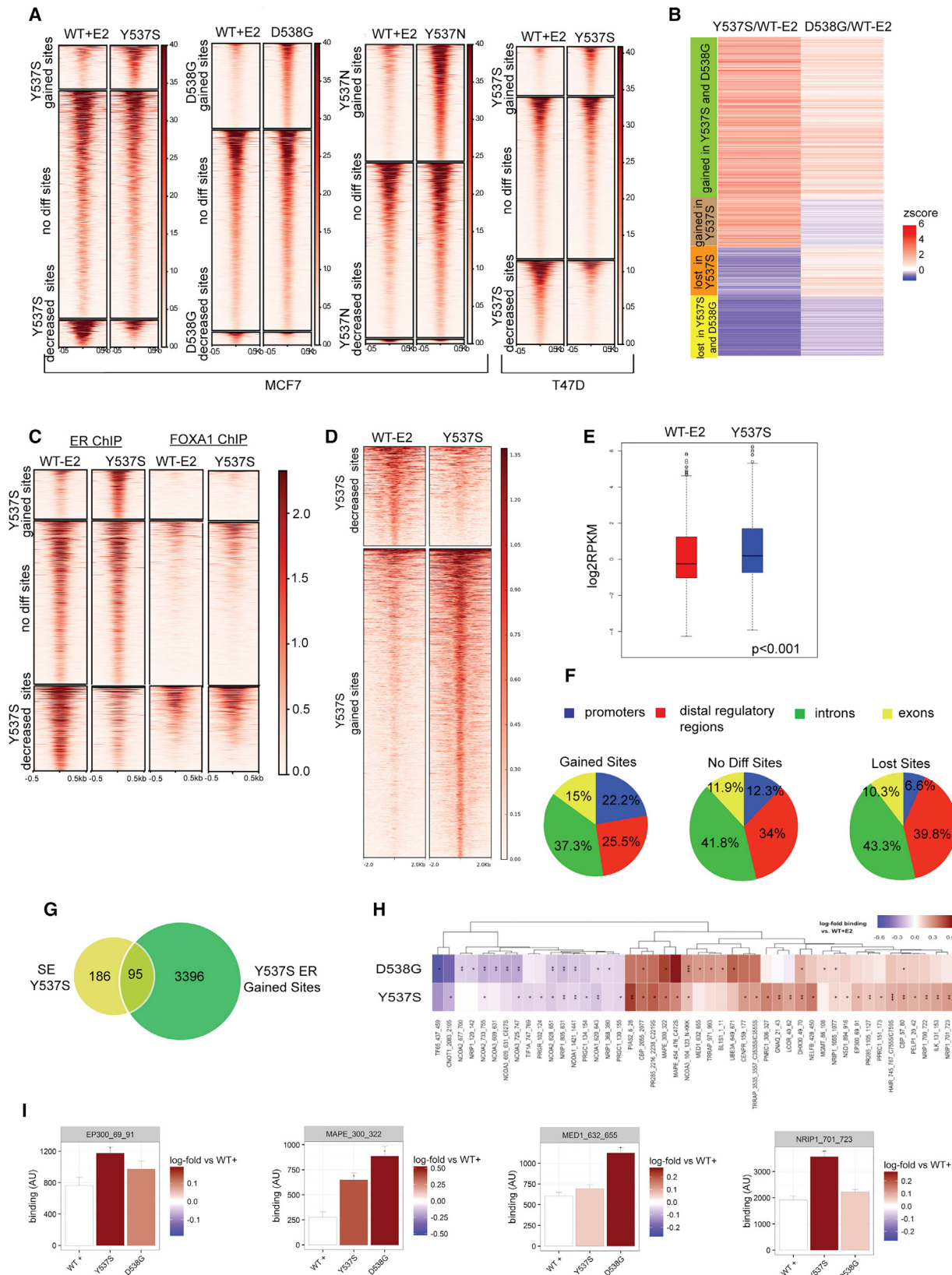
See also Figure S2.

harbor WT ER and 4 patients harbored the Y537S mutation. Similar to the analysis of the first cluster, in a supervised analysis of this cluster we detected a transcriptional profile upregulated in tumors harboring the Y537S mutations. GSEA utilizing custom gene sets of the 100 or 50 top-ranked genes upregulated after induction of the Y537S mutant in the MCF7 cell line were enriched in the Y537S metastatic tumors compared with the WT ER metastatic tumors in the second cluster (NES = 1.4, p < 0.01, and NES = 1.7, p < 0.001, for 100 and 50 top-ranked genes, respectively) (Figure 2C). In addition, the gene sets of the 100 or 50 top-ranked genes upregulated with the induction of the D538G mutant in MCF7 cells were also enriched in the Y537S metastatic tumor samples (NES = 1.5, p < 0.01, and NES = 1.7, p < 0.001, for 100 and 50 top-ranked genes, respectively) (Figure S2D). This is highly consistent with the cell line transcriptome analyses in which the majority of D538G-induced genes were included within the Y537S-induced genes. These

clinical data strongly support the importance of the findings in the cell line models harboring the ER mutants.

We also performed RNA-seq in a series of ER⁺ patient-derived xenografts (PDXs) that were established from four ER⁺ metastatic breast cancer tissue samples. Two of these xenografts harbor a Y537S mutation, as detected by directed droplet digital PCR and RNA-seq. We confirmed ER expression in the xenografts (Figure S2E). In an unsupervised analysis of the RNA-seq of tumors harvested in the first and second passage of the PDX in the presence of E2 supplementation, the Y537S mutant PDX

enrichment score [NES] = 1.44, p < 0.01 and NES = 1.5, p < 0.001 for the 100 and 50 top-ranked genes, respectively) (Figure 2B). In contrast, the gene sets of the 100 or 50 top-ranked genes upregulated with the induction of the Y537S mutant in MCF7 cells were not enriched in the D538G metastatic tumor samples (Figure S2C). This is consistent with the cell model findings in which the majority of the Y537S-induced genes did not overlap with the D538G-induced genes (Figure S1Ed). The second cluster of 67 cases included sites other than liver predominantly. Of these 67 cases, 63 were found to



(legend on next page)

models clustered distinctly from the WT ER PDX models (Figure S3F). GSEA showed that the gene signature of AKT1 activation was the top-ranked enriched signature in the mutant PDXs compared with the WT ER PDXs ($\text{NES} = 1.8$, $p < 0.01$) (Figure S2G). To test for a correlation between the transcriptional changes in the mutant PDX tumor tissues and the ER Y537S mutant cell line models, we constructed a custom gene set for use in GSEA. This gene set consisted of the 100 top-ranked genes induced by the Y537S mutant selected by FC and an FDR < 0.01 . Notably, there was a significant enrichment of 94 of these 100 genes in the Y537S mutant PDX tumors compared with the WT ER tumors ($\text{NES} = 1.14$, $p < 0.01$) (Figure S2H).

Mutant ER Cistromes Are E2 Independent and Distinct from the E2-Dependent WT ER Cistrome

As we found that the transcriptional changes induced by the ER mutants were not restricted to E2-dependent genes, we hypothesized that the ER mutations lead to an altered ER cistrome, and consequently to modulations in the ER transcriptional network. To test this hypothesis and discern which genes are directly regulated by the ER mutants we mapped ER binding globally by performing ER chromatin immunoprecipitation sequencing (ChIP-seq) of the DOX-induced mutant cells in HD conditions, and the WT cells in HD conditions, and after E2 stimulation. As expected from our prior work, the ER ChIP-seq for the WT cells in HD conditions yielded a very low number of binding sites and did not pass our quality control parameters (Carroll et al., 2005). In contrast, the mutant ER was recruited to DNA binding sites in the absence of E2 stimulation, resulting in a total of 35,000 binding sites in MCF7-Y537S mutant cells, 23,676 in Y537N mutant cells, and 11,371 in D538G mutant cells. To confirm that we were detecting the recruitment of mutant ER, we performed HA-ChIP-seq in the presence of DOX, with and without E2 stimulation, and saw a high correlation between the mutant ER cistromes with HA and ER antibodies (Figure S3A). We next performed a differential binding intensity analysis to define sites with up- or downregulated binding intensity. We found that the ER mutations led to the redistribution of ER binding profiles at 24% or more of all binding events. In the MCF7-Y537S cells,

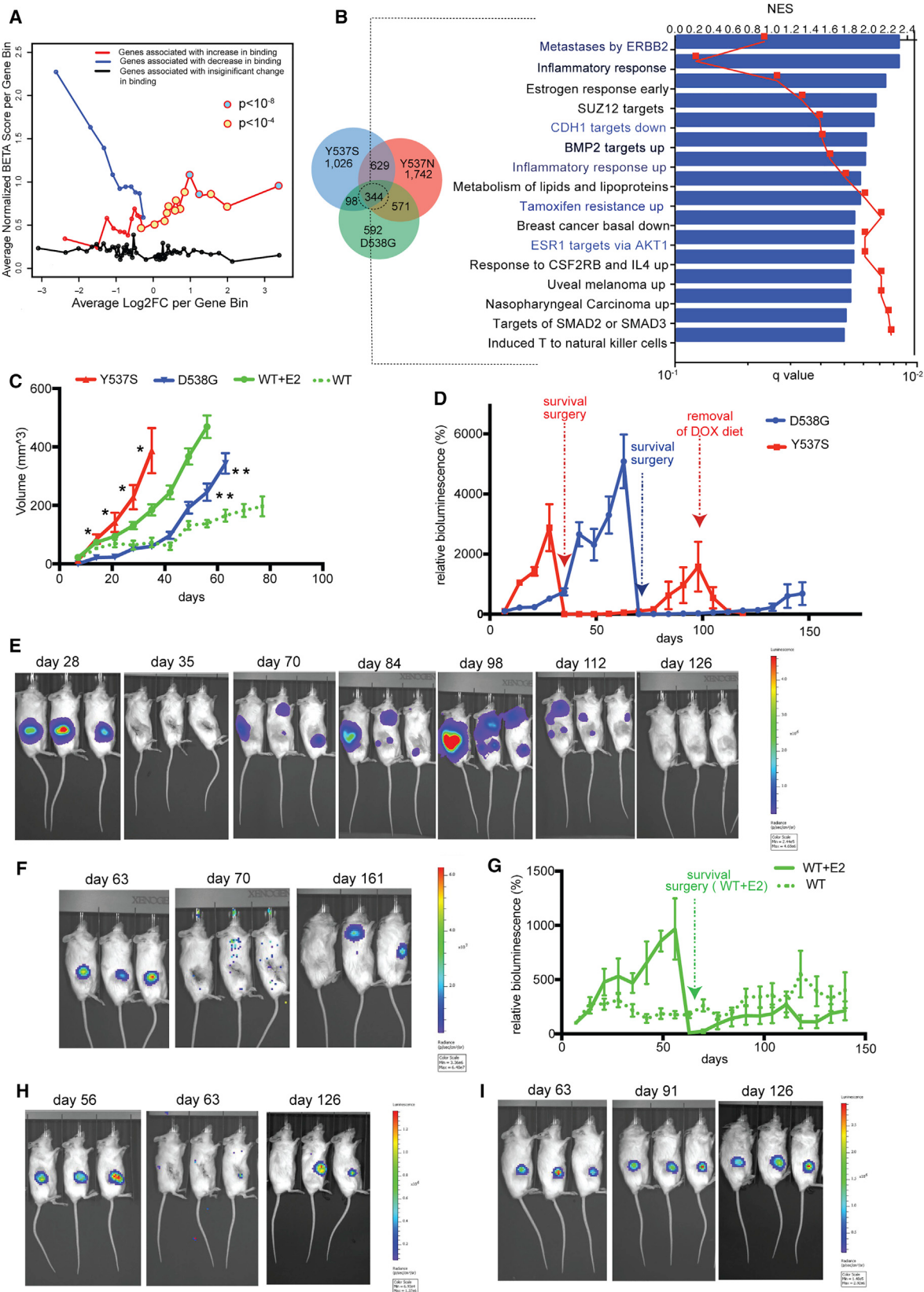
15% of the binding events had increased binding intensity compared with WT ER E2-stimulated cells, and 9% had decreased binding intensity. In the MCF7-D538G cells, 33% of the binding events had increased binding intensity. The E2-independent recruitment and partial redistribution of ER binding events in the presence of the ER mutations were not cell line specific, since the induction of the Y537S mutant in T47D cells led to E2-independent recruitment and redistribution of 45% of all the ER binding events (Figure 3A). When we compared the Y537S and D538G differential binding sites, we saw that 50% of the sites with increased binding intensity, and 20% of the binding sites with decreased intensity overlapped between the Y537S and D538G mutations. Thus, similar to the transcriptional differences between the Y537S and D538G mutations, the two mutations lead to distinct alterations in the ER cistrome (Figure 3B).

Motif analysis revealed that the ER binding motif (ERE) was significantly enriched in all the binding sites, indicative of direct ER binding. The ERE and ERE half-site motifs were the only motifs enriched in the ER mutant gained binding sites. In addition to the ERE, motifs of transcription factors known to be important for ER action, such as FOXA1, AP1, and GRHL2, were enriched in the binding sites common to the WT and mutants. The second most significantly enriched motif in WT ER-selective binding sites common to MCF7 and T47D was FOXA1 (Table S3). In addition, we mapped the Y537S and D538G ER mutant binding without E2 stimulation in cells expressing the mutant ER generated by gene knockin (KI) in MCF7 cells and in the parental WT MCF7 cells following E2 stimulation. Similar to the DOX-inducible cells, we detected E2-independent ER recruitment in the presence of the Y537S and D538G mutations, with a redistribution of 39% and 49% of the ER binding events for the Y537S and D538G mutations, respectively (Figure S3B). Furthermore, motif analysis showed that the mutant-selective sites were enriched in ERE motifs for the Y537S and D538G mutant cells, while the WT-selective were enriched in FOXA1 motifs.

The FOXA1 motif was not significantly enriched in the mutant-selective binding sites, suggesting that FOXA1 may be less essential for mutant-specific ER DNA binding. To test whether FOXA1 was indeed differentially recruited to the

Figure 3. Distinct ER Mutant Cistromes Drive a Unique Transcriptional Network

- (A) Heatmaps of WT ER binding events after estradiol (E2) stimulation compared with ER mutant binding sites in HD conditions for the Y537S, Y537N, and D538G mutations in MCF7 cells and Y537S in T47D cells shown in a horizontal window of ± 0.5 kb from the peak center. Heatmaps depict the sites that are gained in the mutant, not different between the ER mutant and WT ER after estradiol stimulation, and sites lost in the mutant.
 - (B) Heatmap of the ER binding intensity ratios of Y537S mutant in HD conditions over WT mutant after E2 stimulation and D538G mutant in HD conditions over WT mutant after E2 stimulation in the sites gained and lost in Y537S and D538G.
 - (C) Heatmaps of WT ER and Y537S mutant ER binding events and corresponding FOXA1 binding in MCF7 cells showing the ER binding sites selective to the Y537S, shared with WT ER and selective to WT ER, shown in a horizontal window of ± 0.5 kb from the peak center.
 - (D) Heatmaps of the differential H3K27ac binding sites comparing WT cells with E2 stimulation and ER mutant binding sites in HD conditions for the Y537S MCF7 cells. Shown in a horizontal window of ± 2 kb from the peak center.
 - (E) Each box in the boxplot is the cumulative H3K27ac binding overlapping with the Y537S mutant gained ER binding sites in the WT and Y537S mutant MCF7 cells. The y axis represents the reads per kilobase per million (RPKM) reads of DNA. The line in the box represents the median, box limits indicate the first and third quartile, whiskers extend 1.5 the interquartile range from the first and third quartiles, the dots represent outliers.
 - (F) The distribution of the regions of the ER binding sites per category, including the ER binding sites gained in the Y537S cells, sites that are not different from WT ER and the sites lost in the Y537S cells.
 - (G) Venn diagram showing the overlap between the super-enhancer (SE) regions in Y537S MCF7 cells and the Y537S gained ER binding sites.
 - (H) Heatmap of ER mutant co-regulator binding in HD conditions compared with WT ER co-regulator binding after E2 treatment. * $p < 0.05$, ** $p < 0.005$, *** $p < 0.001$.
 - (I) Bar graphs show binding affinity levels for peptides of the ER co-regulators EP300, MAPE, MED1, and NRIP1 in WT ER + E2 stimulation and Y537S and D538G mutant ER in HD conditions in MCF7 cells. Error bars represent SEM, $n = 3$.
- See also Figure S3 and Tables S3 and S4.



(legend on next page)

mutant-selective ER binding sites, we performed FOXA1 ChIP-seq in WT ER cells with E2 stimulation and in the Y537S mutant cell without E2 stimulation. Co-occupancy analyses showed a significant enrichment of FOXA1 binding events within the WT ER-specific cistrome, and significantly lower FOXA1 binding events in the ER mutant-specific cistrome ($p < 0.0005$) (Figure 3C). Nonetheless, FOXA1, which is enriched in the non-differential binding sites, and is also upregulated by the induction of the ER mutants, remains essential for mutant and WT ER cell proliferation, as demonstrated by silencing of FOXA1 (Figures S3C and S3D). Albeit in the presence of the Y537S mutant in HD conditions, the effect of FOXA1 silencing on cell proliferation was not statistically significant.

To gain insight into the chromatin modifications at the ER mutant gained binding sites, we performed ChIP-seq for the active histone mark H3K27ac in WT ER MCF7 cells with E2 stimulation cells and mutant ER cells in HD conditions. A substantial number of H3K27ac binding sites were gained in the mutant cells (2,379 sites, $\log_2 FC > 0.5$), and these sites were enriched in ERE motifs ($p = 1 \times 10^{-8}$) in addition to E2F ($p = 1 \times 10^{-16}$) and ETS ($p = 1 \times 10^{-9}$) motifs (Figure 3D). The latter two were the top motifs. Moreover, the ER binding sites gained in the presence of the mutations were more likely to be centered at regions of active chromatin in the Y537S mutant cells compared with the WT cells as indicated by the increased levels of H3K27ac at these sites in the mutant cells compared with the WT cells (Figure 3E). In addition, the ER binding sites gained in the Y537S mutant cells are more likely than those of the other categories to occur in promoter regions and >30% of the super-enhancers detected in the Y537S mutant cells overlapped with the mutant gained binding sites (Figures 3F and 3G).

Our results indicate that the ER binding sites gained in the presence of the mutations occur at transcriptionally active regions. However, we did not identify co-occupancy of a specific pioneer factor in these sites. We therefore hypothesized that the altered conformation of the ER mutants and unique co-regulator binding might contribute to the enhanced mutant ER binding in these sites. To test this hypothesis we screened mutant ER compared with WT ER co-regulator interactions using the Microarray Assay

for Real-time Co-regulator-Nuclear receptor interaction (Koppen et al., 2009). We identified 58 E2 dependent co-regulator peptides in the presence of WT ER. The majority of these E2-dependent co-regulators peptides interacted with similar binding levels to the apo-mutant ER (55 for Y537S and 48 for D538G), consistent with constitutive binding of multiple co-regulators (Figure S3E). Among these co-regulators are known ER co-activators such as NCOA3. Comparison of apo-mutant to E2-stimulated WT ER co-regulator interactions revealed a number of significantly enhanced apo-mutant interactions (24 for Y537S and 11 for D538G). These include, among others, the ER co-activators EP300, MED1, and NRIP1 (Rosell et al., 2014; Kornberg, 2005; Yi et al., 2015) (Figures 3H and 3I; Table S4). Comparison of the apo-Y537S versus apo-D538G mutant revealed mutant-selective co-regulator peptide interactions (Figure S3F). These results provide an indication that the co-regulator peptide-mutant ER interaction landscape is allele selective and differs from that of WT ER. However, studies to further investigate the effect of the mutant structure on multiple co-regulator interactions are needed to clarify whether this is simply an indication of subtle structural differences between the alleles or the mediator of the differences in cistromes and transcriptomes.

The Mutant ER Cistrome Mediates Transcriptional Changes that Promote a Metastatic Phenotype

We next applied the Binding and Expression Target Analysis (BETA) algorithm, which assigns a BETA score for each gene based on the distance between the transcription start site of a gene and the peak of the transcription factor binding sites (Wang et al., 2013), to test for a correlation between the redistribution of the mutant ER recruitment and the transcriptional differences between mutant ER and WT ER. We found a statistically significant correlation between the BETA scores for the Y537S- and WT-selective binding sites and the differential gene expression between E2-stimulated WT ER and non-stimulated Y537S-ER. Whereas, for the shared binding sites there was no significant correlation (Figure 4A). Similarly, we detected a positive correlation between the D538G mutant-selective binding site BETA scores and the differential gene expression

Figure 4. The Mutant-Specific Transcriptional Program Promotes a Metastatic Phenotype

- (A) Correlation of the Y537S mutant-specific cistrome and differential gene expression. The red line represents the genes (2,598 genes) that have Y537S mutant unique peaks ($\log_2 FC > 1$; 3,491 peaks). The blue line represents the genes (966 genes) that have peaks associated with them that were unique to WT ER ($\log_2 FC < -1$; 2,180 peaks). The black line represents the genes (5,250 genes) associated with peaks common to mutant and WT ER ($-1 < \log_2 FC < 1$). The x axis is the $\log_2 FC$ of the genes in mutant condition versus WT condition. The y axis is the average normalized BETA score per gene bin.
 - (B) Overlap of the genes with a ranked product <0.001 determined by BETA using the mutant (Y537S, Y537N, and D538G) unique binding sites and gene sets significantly enriched in the 344 overlapping genes using ranked gene set enrichment analysis (GSEA). The red line in the graph represents the q value and the blue bars represent the NES.
 - (C) Tumor growth of orthotopic xenografts of MCF7 cells expressing the indicated ER mutants or WT MCF7 cells with estradiol (E2) pellets and without E2 supplements prior to the survival surgery. The y axis represents the tumor volume measured by calipers. Comparison of Y537S to D538G mutant cells was statistically significant, * $p < 0.05$, for this comparison. ** $p < 0.005$ in the comparison of the WT xenografts without E2 to all other conditions.
 - (D) Tumor growth of the orthotopic xenografts of MCF7 cells expressing the Y537S or D538G mutation from the time of the intra-mammary injections of the cells through the survival surgery and monitoring of local recurrence and distant metastases (mets).
 - (E) Representative pictures of the mice with the Y537S xenografts. Survival surgery was performed on day 35 and the DOX diet was discontinued on day 98.
 - (F) Representative pictures of the mice with the D538G xenografts. The survival surgery was performed on day 70.
 - (G) Tumor growth of the orthotopic xenografts of WT MCF7 cells with E2 (WT + E2) or without E2 (WT) supplements from the time of the intra-mammary injections of the cells through the survival surgery and monitoring of local recurrence and distant mets.
 - (H) Representative pictures of the mice with WT MCF7 cells + E2 pellets. The survival surgery performed on day 63.
 - (I) Representative pictures of the mice with WT MCF7 cells without E2 pellets. Survival surgery was not performed in these mice. Error bars in (C-E) represent SEM, six to eight mice were included in each arm.
- See also Figure S4 and Table S5.

between E2-stimulated WT ER and non-stimulated D538G ER (**Figure S4A**). Since there was a limited number of WT-selective binding sites in the D538G mutant cells we did not perform this analysis for these binding sites. Taken together, these correlations imply that the transcriptional changes induced by mutant ER in HD conditions are driven by the ligand-independent redistribution of mutant ER cistromes.

By integrating the BETA scores of the ER mutant-selective binding sites and the differential gene expression between the WT cells + E2 stimulation versus mutant cells in HD conditions and selecting genes that have a rank product of <0.01 , we identified the genes that are directly upregulated by the ER mutants. We compared the genes upregulated by the three mutants (Y537S, Y537N, and D538G) and found 344 overlapping genes (**Figure 4B**) (genes listed in **Table S5**). GSEA identified genes upregulated in metastases driven by ERBB2 (NES = 2.3, $q = 0.02$) as the top-ranked gene set enriched in the overlapping genes upregulated by the ER mutants. Other gene sets that were significantly enriched consist of a number of gene sets important for the metastatic process, including: gene sets of inflammatory response (NES = 2.3, $q = 0.01$), genes downregulated by CDH1 (NES = 2, $q = 0.04$), genes upregulated by BMP2 (NES = 2, $q = 0.04$), and genes upregulated in TAM resistance (NES = 1.9, $q = 0.06$). The gene set of ER targets via AKT1 upregulation was also significantly enriched in the ER mutant upregulated genes and is in keeping with the top gene set enriched in the Y537S PDX models.

To functionally test the mutant pro-metastatic phenotype we generated orthotopic xenografts with the Y537S and D538G DOX-inducible cells stably infected with luciferase in ovariectomized mice treated with a DOX diet without E2 supplement. As controls, we used MCF7 cells expressing WT ER in ovariectomized mice with and without E2 pellets. The mice were monitored for mets before and after survival surgery to remove the primary tumor. The mammary tumor growth was significantly greater in the Y537S mutant cells compared with the D538G mutant cells. Growth of the WT ER-expressing tumors in the presence of E2 was not significantly different from the mutant ER-expressing tumors in the absence of E2 (**Figure 4C**), whereas, growth of WT ER-expressing tumors in the absence of E2 was significantly lower compared with the ER mutant and WT + E2 tumor growth (**Figure 4C**). All six mice harboring the Y537S ER-expressing xenografts grew primary tumors within 2 weeks and developed mets within 70 days from the injection of the cells and 25 days from the survival surgery. The mets were dependent on the Y537S mutant, as removal of the DOX diet led to rapid regression of the mets (**Figures 4D**, **4E**, and **S4B–S4D**). The D538G tumors developed mets, but with a longer latency (on day 147 from the injection of the cells five of the eight mice were found to have metastases) (**Figures 4D** and **4F**). Although four of the eight mice injected with WT cells and treated with supplemental estrogen developed local recurrences after survival surgery, not one developed mets (WT versus Y537S, $p = 0.0002$, and WT versus D538G, $p = 0.007$, chi-square test) (**Figures 4G** and **4H**). Survival surgery was not performed in the mice with WT ER xenografts in the absence of E2 since the tumors did not reach the predefined threshold volume for surgery. Similar to the WT ER cells with E2 supplement, these mice did not develop mets (**Figures 4G** and **4I**).

Collectively, these results demonstrate that the ER mutations lead to a reprogrammed transcriptional network that promotes metastases, and this phenotype is more pronounced in the Y537S compared with the D538G mutation.

CRISPR Knockout Screen Identifies Genes Essential for Mutant ER Growth

To investigate genes that are essential for mutant ER E2-independent growth, we performed genome-wide CRISPR-Cas9 knockout screens in the T47D-Y537S cells in HD conditions and control parental WT ER cells in FM conditions using two libraries targeting over 18,000 protein coding genes consisting of over 180,000 guide RNAs (gRNAs). The negatively and positively selected genes were identified by calculating the gene essentiality score, defined as the beta score, using MAGeCK-VISPR ([Li et al., 2015](#)). Similar to our screens in WT ER breast cancer cells, the top genes that were positively selected in the ER mutant library screen are tumor suppressors, such as *NF1*, *TSC1*, *TSC2*, *PTEN*, and *CSK*. In addition, *MYH9* and *CBFB*, two genes previously found as mutated in ER⁺ breast cancers, were also among the top-ranked positively selected genes ([Ellis et al., 2012](#)). As expected, among the top negatively selected genes, i.e., the essential genes, were genes that are known driver genes of ER⁺ breast cancer, such as *GATA3* (beta = -2), *TFAP2C* (beta = -1.8), *MTOR* (beta = -1.7), *MYC* (beta = -1.3), and *ESR1* itself (beta = -1.1) (**Figure 5A**). These genes were also essential in the T47D WT cells in FM conditions (**Figure 5B**). In addition, *CCND1* (beta = -1.6) and *CDK4* (beta = -1.8) remained essential genes in the mutant cells. This is consistent with a retrospective clinical study in which patients with ER mutations remained sensitive to CDK4/6 inhibitors ([Fribbens et al., 2016](#)). We confirmed that the ER mutant-expressing cell lines retained sensitivity to palbociclib, a CDK4/6 inhibitor (**Figure S5A**). In addition, a number of the ER co-regulators, such as *NCOA3*, *EP300*, *MED1*, and *MEN1*, which we found to interact with the apo-mutant ER, were essential in the mutant cells. Notably, we observed increased apo-ER mutant binding to *EP300* and *NCOA3* compared with E2-stimulated WT ER, and both of these co-regulators were more essential in the Y537S mutant cells compared with the WT cells (*EP300*: WT beta = -0.1, mutant beta = -1; *NCOA3*: WT beta = -0.1, mutant beta = -0.5).

To prioritize essential genes that are selective or retained in cells expressing mutant ER and are directly upregulated by mutant ER, we used a rank-product algorithm to aggregate rankings of scores from the output of MAGeCK-VISPR and the geometric mean of the gene rankings from four of the BETA analysis results (D538G, Y537N, and Y537S from MCF7 cells and Y537S from T47D cells) (**Table S6**; **Figure 5C**). *TFAP2C* was found to be the top gene in this ranking (rank product FDR = 0.036). *TFAP2C* was essential in the WT ER CRISPR screen in FM conditions, but the essentiality score was more significant in the presence of the Y537S mutant in HD conditions (WT ER beta = -0.9 FDR = 0.01, Y537S beta = -1.8 FDR < 0.0001). In addition, the Y537S ER binding site in the promoter region of *TFAP2C* overlapped with a super-enhancer region (**Figure 5D**). *TFAP2C* is a regulator of ER transcriptional activity and luminal differentiation ([Cyr et al., 2015](#)). Moreover, we recently showed that *TFAP2C* expression was highly associated with decreased progression free survival

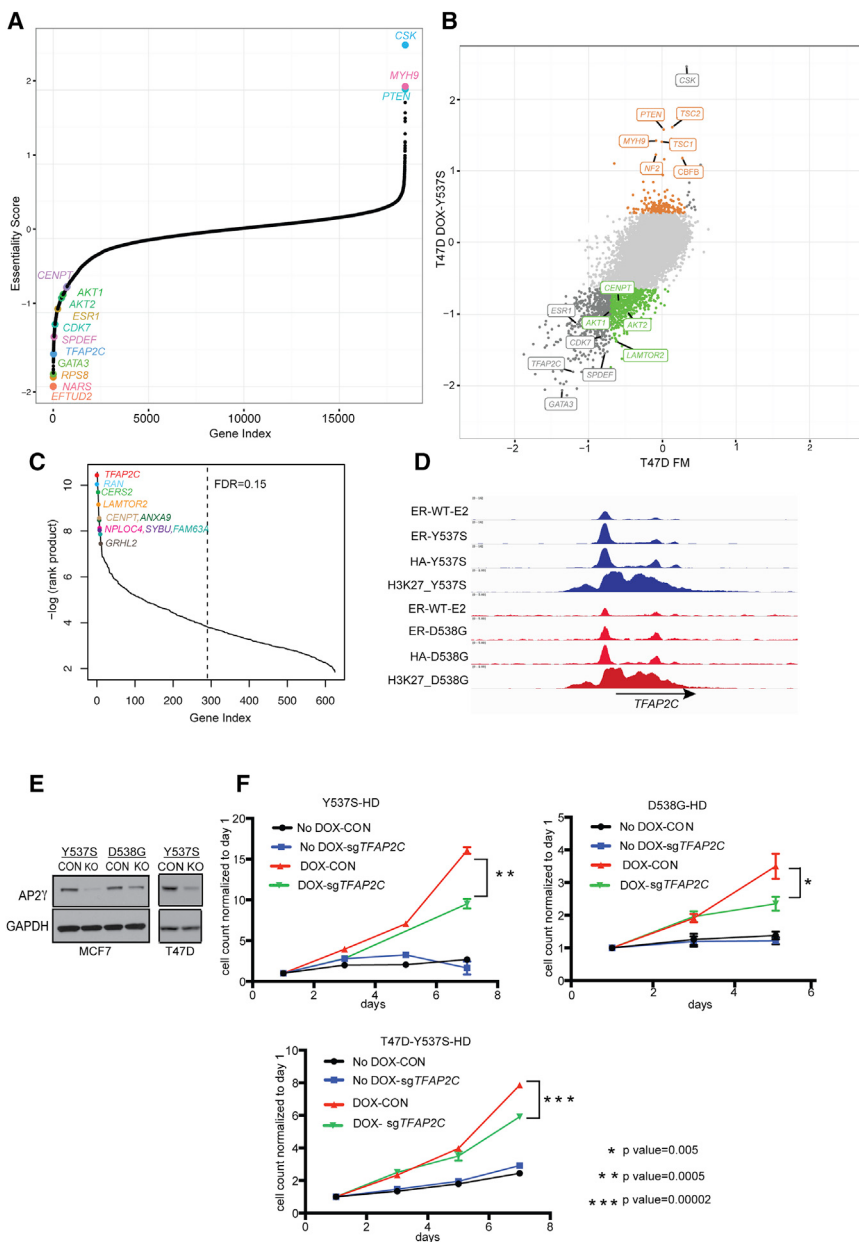


Figure 5. CRISPR Screen Identifies ER Mutant Essential Genes

(A) Essentiality scores from the CRISPR screen in T47D-Y537S mutant cells grown in HD conditions. (B) Comparison of beta scores of CRISPR-Cas9 library screens in Y537S-ER mutant cells in HD conditions versus library screen in WT ER cells in FM conditions. Dark gray dots, genes that are essential for both WT ER and mutant ER; green, uniquely essential for mutant ER; orange, uniquely positively selected in mutant ER; and light gray, not significant in the mutant cells ($FDR < 0.05$). (C) $-\log$ rank product values integrating the beta essentiality scores and the geometric mean of the gene rankings from at least three of four BETA analysis results from the Y537S, D538G, and Y537N MCF7 cells and T47D Y537S cells. (D) ChIP-seq tracks showing ER, HA, and H3K27 acetylation binding at the TFAP2C promoter region in WT cells with E2 treatment and mutant cells in HD conditions. (E) Immunoblotting for AP2 γ in control (CON) cells and cells with CRISPR-Cas9 suppression of TFAP2C (KO). (F) Cell proliferation studies in HD conditions of WT and Y537S or D538G mutant (DOX treated) control cells and after suppression of TFAP2C using CRISPR-Cas9. Error bars represent \pm SEM, $n = 3$. See also Figure S5 and Table S6.

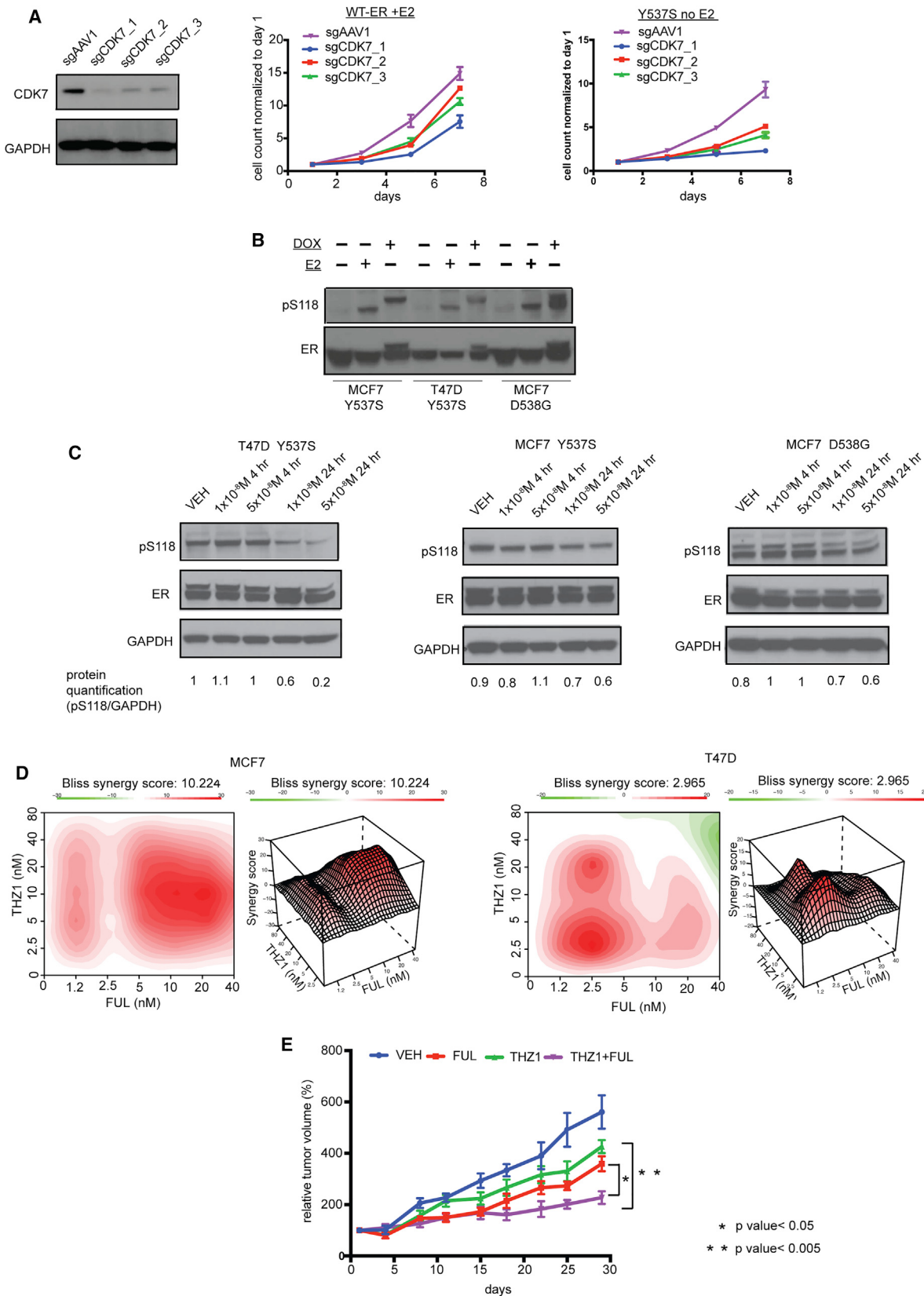
ER-Y537S beta score = -1.3 , $FDR < 0.0001$), and a CDK7 small-molecule inhibitor, THZ1, was well characterized (Kwiatkowski et al., 2014). CDK7 is a component of the general transcription factor IIH complex, which phosphorylates the C-terminal domain of RNAP polymerase II. In addition to its function in transcriptional regulation, CDK7 functions as a CDK-activating kinase (CAK) for CDK1, 2, 4, and 6, and has also been shown to modulate ER activity through serine 118 (S118) phosphorylation (Chen et al., 2000; Fisher and Morgan, 1994; Glover-Cutter et al., 2009; Larochelle et al., 2007). S118 is a major phosphory-

lation site within the N-terminal domain transcription activation 1, and mutations in this site were shown to impair transactivation by ER (Ali et al., 1993). CDK7 silencing with CRISPR-Cas9 gRNAs resulted in suppressed proliferation in both WT ER cells in FM and mutant ER cells in HD conditions (Figures 6A, S6A, and S6B).

We next tested the effect of THZ1 on cell growth. WT and ER mutant MCF7 and T47D cells were responsive to THZ1 treatment, and the IC_{50} values were comparable between WT and mutant ER cells (Figure S6C). THZ1 covalently modifies CDK7 at residue C312 outside of the kinase domain, and previous studies have shown that THZ1 inhibits RNAPII CTD phosphorylation and CAK activity in leukemia cell lines (Kwiatkowski et al., 2014). More recently, THZ1 was shown to inhibit RNAPII CTD phosphorylation and ER phosphorylation at S118 in MCF7 cells

in metastatic ER $^+$ breast cancer (Jeselsohn et al., 2016). To validate that TFAP2C is an ER mutant transcriptional target, and an essential gene for mutant cell growth in HD conditions, we first confirmed mutant-induced upregulation of TFAP2C mRNA and protein levels (Figures S5B and S5C). Next, we showed that silencing of TFAP2C by CRISPR-gRNAs decreased E2-independent proliferation of Y537S and D538G mutant cells (Figures 5E and 5F). We also showed that TFAP2C suppression did not affect ER expression (Figure S5D). Thus, TFAP2C is upregulated by the ER mutants and is essential for E2-independent mutant ER cell growth.

We next turned to validate the effects of essential genes with available small-molecule inhibitors, as these are potential drug targets. CDK7 was essential in both ER mutant and WT ER-expressing cells (WT ER beta score = -0.8 , $FDR = 0.017$;



(legend on next page)

with WT ER and an ER Y537S KI allele (Harrod et al., 2016). Here, we examined the effect of THZ1 on E2-independent Y537S and D538G mutant ER S118 phosphorylation. Since the mutant ER is HA tagged in our cell line models we could differentiate between WT ER and mutant ER in a western blot, which allowed us to discern selective E2-independent phosphorylation of the Y537S and D538G ER mutants. As expected, we did not detect WT ER S118 phosphorylation in E2-deprived conditions. Interestingly, however, in the presence of the D538G mutant in E2-deprived conditions we detected S118 phosphorylation of the D538G mutant ER and WT ER (Figure 6B). Phosphorylation of WT ER was not seen with the Y537S mutant, and may suggest that the D538G mutant has a higher propensity to heterodimerize with WT ER. This could potentially explain some of the phenotypic differences between the Y537S and D538G mutations, although further studies are needed to validate this hypothesis. We next tested the effect of THZ1 on ER mutant E2-independent S118 phosphorylation, and found dose- and time-dependent inhibition of Y537S and D538G S118 phosphorylation (Figure 6C). Gene expression analysis of Y537S mutant cells treated with THZ1 at 24 hr showed that the key pathways that were inhibited were related to the ErbB/PI3K/MTOR pathway, which is in line with the key pathways enriched in the genes upregulated by the ER mutations, suggesting that THZ1 is targeting the ER mutant transcriptional network (Figure S6D).

We next studied the combination of THZ1 with FUL in cell culture and *in vivo*. We detected significant synergism of this combination in MCF7 and T47D WT ER and mutant Y537S in the DOX-inducible cell lines as well as the Y537S KI cell line (Figures 6D and S6E). Orthotopic xenografts of MCF7 cells expressing the Y537S mutant demonstrated that the combination of THZ1 with FUL had improved efficacy in inhibiting tumor growth compared with either single agent (Figure 6E). These results support the potential of this combination as a therapeutic strategy to overcome endocrine resistance caused by the ER mutants.

DISCUSSION

Constitutively active somatic mutants in the ER LBD have emerged as a frequent mechanism of endocrine therapy resistance in patients with metastatic ER⁺ breast cancers. Whether these mutant alleles simply mimic the actions of estrogen-bound ER or express additional neomorphic or allele-specific properties could have important therapeutic implications for patients. We undertook a systematic approach to answer these questions and to identify potential targets for therapies in metastatic breast cancers driven by these ER mutants.

By integrating RNA-seq and ChIP-seq data we show that the ER mutants lead to E2-independent chromatin binding and distinct cistromes and allele-specific transcriptional programs compared with the E2-stimulated WT ER. The mechanistic basis for the allele-selective chromatin recruitment is not well understood, and we hypothesize that this may be due to allele-selective interactions with co-regulators, or other transcription factors that ultimately mediate differences in chromatin binding. Additional biophysical studies will be needed to test this hypothesis.

Importantly, examination of the mutant allele-specific transcriptional programs reveals that these programs are enriched in genes and pathways that mediate growth factor signaling and promote metastases. These findings provide a mechanistic basis by which the ER mutants engender endocrine resistance and may explain the metastatic propensity and poor overall survival of patients with metastatic breast cancers harboring these mutants.

We were able to demonstrate the relevance of the allele-specific mutant ER transcriptional signatures developed in model cell lines in PDXs and a large set of ER⁺ metastatic tumor biopsies. In this metastatic biopsy cohort we also confirmed our previous findings from a smaller cohort (Merenbakh-Lamin et al., 2013) of enrichment of the D538G mutant allele specifically in liver metastases. The molecular mechanism of this organotropism is unknown and warrants further study. Consistent with our findings of ER mutant allele-specific programs, a recent analysis of the BOLERO2 clinical trial suggested that patients with the Y537S mutant allele may have worse outcomes compared with patients whose tumors harbor the D538G mutation (Chandarlapaty et al., 2016). Additional studies with larger numbers of patients harboring these ER mutations will be needed to determine the clinical differences among the various mutant alleles, including responses to specific endocrine treatments and prognosis.

We used a highly efficient genome-wide CRISPR KO library to detect genes essential for the E2-independent growth of ER mutant-expressing breast cancer cells. As these ER mutants are constitutively active, it is not surprising that many of the essential genes identified in the screen are known drivers of ER⁺ breast cancers. In addition, genes such as *TFAP2C*, and a number of others that are directly upregulated by the ER mutants, were shown to be essential for the E2-independent growth driven by the mutations.

In summary, we have comprehensively profiled the epigenetic and transcriptional programs regulated by ER-LBD mutations found in endocrine therapy-resistant ER⁺ breast cancer and provide mechanistic insights into the allele-specific roles played by these mutations in promoting hormone-independent metastatic

Figure 6. CDK7 Is Essential for Mutant ER Constitutive Activity

(A) Immunoblotting for CDK7 in AAV1-control (AAV1-con) cells, and cells with CDK7 silencing with three different CRISPR-Cas9 gRNAs. Cell proliferation studies of T47D WT ER cells with AAV1-con and CDK7 silencing in FM and Y537S mutant cells in HD conditions.

(B) Immunoblotting for ER and phospho-ER at serine 118 (S118) in WT cells (−DOX) in HD and E2-stimulated conditions and Y537 or D538G mutant (+DOX) ER in HD conditions.

(C) ER and pS118 levels by immunoblotting after vehicle (VEH) and THZ1 treatment at 4 hr and 24 hr with increasing doses.

(D) 2D and 3D synergy maps of THZ1 and FUL treatment combination in MCF7 (left) and T47D (right) cells expressing the Y537S mutation.

(E) Growth curves of orthotopic xenografts of the MCF7-Y537S cells after treatment with VEH, FUL, THZ1, or the combination of FUL and THZ1. Error bars represent ±SEM, n = 8.

See also Figure S6.

growth. Our ability to validate these findings from cell culture models in a large cohort of metastatic biopsies offers hope that the therapeutic targets identified in the models will be able to be translated to the clinic to improve outcomes for patients with metastatic ER⁺ breast cancers harboring these mutations.

STAR★METHODS

Detailed methods are provided in the online version of this paper and include the following:

- KEY RESOURCES TABLE
- CONTACT FOR REAGENT AND RESOURCE SHARING
- EXPERIMENTAL MODEL AND SUBJECT DETAILS
 - Cell Lines
 - In Vivo Animal Studies
 - Human Tissue Studies
- METHOD DETAILS
 - Generation of DOX-Inducible WT and Mutant ER Cells
 - Generation of Transcription Activator Like Nucleases (TALEN) Mediated Mutant Cells
 - Proliferation Assays
 - Western-Blotting
 - Chromatin Immunoprecipitation (ChIP)-Sequencing
 - RNA Sequencing
 - Co-Regulator Interaction Profiling
 - CRISPR Knock-Out Library Screen
 - Generation of Single CRISPR/Cas9 Knock-Out Cells
 - Drug Synergy Studies
- QUANTIFICATION AND STATISTICAL ANALYSIS
 - RNA Sequencing Analysis
 - ChIP Sequencing Analysis
 - CRISPR/CAS9 Library Screen Analysis
 - Drug Synergy Analysis
- DATA AVAILABILITY

SUPPLEMENTAL INFORMATION

Supplemental Information includes six figures and six tables and can be found with this article online at <https://doi.org/10.1016/j.ccr.2018.01.004>.

ACKNOWLEDGMENTS

This work was supported in part by grant from the NIH K08 CA191058-03 (to R.J.), the Claudia Adams Barr Program for Innovative Cancer Research (to R.J.), NCI grant P50 CA168504 (SPORE) Career Development Award (to R.J.), a Susan G. Komen Leadership Grant (to M.B.), and NIH P01CA080111 (to M.B.).

AUTHOR CONTRIBUTIONS

Conceptualization, M.B., R.J., and G.B.; Methodology, R.J., G.B., T.X., and J.S.B.; Software, M.C., W. Li, A.F., X.Q., H.L., and X.S.L.; Formal Analysis, M.B., R.J., M.C., M.P., W. Li, A.F., N.W., O.C., and R.H.; Investigation, R.J., M.P., M.C., J.S.B., T.X., W. Liu, A.N., K.A.H., G.B., P.R., D.M., and R.H.; Resources, J.S.B., N.G., T.Z., N.W., E.P.W., and J.Z.; Data Curation, M.P. and M.C.; Writing – Original Draft, R.J. and M.B.; Writing – Review & Editing, all authors; Visualization, R.J., M.C., M.P., W. Li, and A.F.; Supervision, R.J., M.B., N.W., H.L., P.R., E.P.W., and J.Z.

DECLARATION OF INTERESTS

G.B. is an employee and shareholder of Celgene. R.H. is an employee of Pamlene International B.V. N.S.G., T.Z., and N.K. are inventors on a patent appli-

cation covering THZ1, which is licensed to a company co-founded by N.S.G. N.W. is a shareholder of Foundation Medicine, is a consultant for Novartis and receives research support from Novartis and Merck. All other authors have no competing financial interests.

Received: July 18, 2017

Revised: November 2, 2017

Accepted: January 9, 2018

Published: February 12, 2018

REFERENCES

- Ali, S., Metzger, D., Bornert, J.M., and Chambon, P. (1993). Modulation of transcriptional activation by ligand-dependent phosphorylation of the human oestrogen receptor A/B region. *EMBO J.* 12, 1153–1160.
- Bailey, T.L., Johnson, J., Grant, C.E., and Noble, W.S. (2015). The MEME suite. *Nucleic Acids Res.* 43, W39–W49.
- Carroll, J.S., Liu, X.S., Brodsky, A.S., Li, W., Meyer, C.A., Szary, A.J., Eeckhoute, J., Shao, W., Hestermann, E.V., Geistlinger, T.R., et al. (2005). Chromosome-wide mapping of estrogen receptor binding reveals long-range regulation requiring the forkhead protein FoxA1. *Cell* 122, 33–43.
- Chandarlapat, S., Chen, D., He, W., Sung, P., Samoil, A., You, D., Bhatt, T., Patel, P., Voi, M., Gnani, M., et al. (2016). Prevalence of ESR1 mutations in cell-free DNA and outcomes in metastatic breast cancer: a secondary analysis of the BOLERO-2 clinical trial. *JAMA Oncol.* 2, 1310–1315.
- Chen, D., Riedl, T., Washbrook, E., Pace, P.E., Coombes, R.C., Egly, J.M., and Ali, S. (2000). Activation of estrogen receptor alpha by S118 phosphorylation involves a ligand-dependent interaction with TFIID and participation of CDK7. *Mol. Cell* 6, 127–137.
- Cyr, A.R., Kulak, M.V., Park, J.M., Bogachek, M.V., Spanheimer, P.M., Woodfield, G.W., White-Baer, L.S., O’Malley, Y.Q., Sugg, S.L., Olivier, A.K., et al. (2015). TFAP2C governs the luminal epithelial phenotype in mammary development and carcinogenesis. *Oncogene* 34, 436–444.
- Dobin, A., Davis, C.A., Schlesinger, F., Drenkow, J., Zaleski, C., Jha, S., Batut, P., Chaisson, M., and Gingeras, T.R. (2013). STAR: ultrafast universal RNA-seq aligner. *Bioinformatics* 29, 15–21.
- Early Breast Cancer Trialists’ Collaborative Group, Peto, R., Davies, C., Godwin, J., Gray, R., Pan, H.C., Clarke, M., Cutler, D., Darby, S., McGale, P., et al. (2012). Comparisons between different polychemotherapy regimens for early breast cancer: meta-analyses of long-term outcome among 100,000 women in 123 randomised trials. *Lancet* 379, 432–444.
- Ellis, M.J., Ding, L., Shen, D., Luo, J., Suman, V.J., Wallis, J.W., Van Tine, B.A., Hoog, J., Goiffon, R.J., Goldstein, T.C., et al. (2012). Whole-genome analysis informs breast cancer response to aromatase inhibition. *Nature* 486, 353–360.
- Fanning, S.W., Mayne, C.G., Dharmarajan, V., Carlson, K.E., Martin, T.A., Novick, S.J., Toy, W., Green, B., Panchamukhi, S., Katzenellenbogen, B.S., et al. (2016). Estrogen receptor alpha somatic mutations Y537S and D538G confer breast cancer endocrine resistance by stabilizing the activating function-2 binding conformation. *eLife* 5, <https://doi.org/10.7554/eLife.12792>.
- Feng, J., Liu, T., Qin, B., Zhang, Y., and Liu, X.S. (2012). Identifying ChIP-seq enrichment using MACS. *Nat. Protoc.* 7, 1728–1740.
- Fisher, R.P., and Morgan, D.O. (1994). A novel cyclin associates with MO15/CDK7 to form the CDK-activating kinase. *Cell* 78, 713–724.
- Fribbens, C., O’Leary, B., Kilburn, L., Hrebien, S., Garcia-Murillas, I., Beaney, M., Cristofanilli, M., Andre, F., Loi, S., Loibl, S., et al. (2016). Plasma ESR1 mutations and the treatment of estrogen receptor-positive advanced breast cancer. *J. Clin. Oncol.* 34, 2961–2968.
- Glover-Cutter, K., Laroche, S., Erickson, B., Zhang, C., Shokat, K., Fisher, R.P., and Bentley, D.L. (2009). TFIID-associated Cdk7 kinase functions in phosphorylation of C-terminal domain Ser7 residues, promoter-proximal pausing, and termination by RNA polymerase II. *Mol. Cell. Biol.* 29, 5455–5464.
- GTEx Consortium (2013). The genotype-tissue expression (GTEx) project. *Nat. Genet.* 45, 580–585.
- Harrod, A., Fulton, J., Nguyen, V.T., Periyasamy, M., Ramos-Garcia, L., Lai, C.F., Metodieva, G., de Giorgio, A., Williams, R.L., Santos, D.B., et al.

- (2016). Genomic modelling of the ESR1 Y537S mutation for evaluating function and new therapeutic approaches for metastatic breast cancer. *Oncogene* 36, 2286–2296.
- Ianevski, A., He, L., Aittokallio, T., and Tang, J. (2017). SynergyFinder: a web application for analyzing drug combination dose-response matrix data. *Bioinformatics* 33, 2413–2415.
- Jeselsohn, R., Yelensky, R., Buchwalter, G., Frampton, G., Meric-Bernstam, F., Gonzalez-Angulo, A.M., Ferrer-Lozano, J., Perez-Fidalgo, J.A., Cristofanili, M., Gomez, H., et al. (2014). Emergence of constitutively active estrogen receptor-alpha mutations in pretreated advanced estrogen receptor-positive breast cancer. *Clin. Cancer Res.* 20, 1757–1767.
- Jeselsohn, R., Barry, W.T., Migliaccio, I., Biagioli, C., Zhao, J., De Tribolet-Hardy, J., Guarducci, C., Bonechi, M., Laing, N., Winer, E.P., et al. (2016). TransCONFIRM: identification of a genetic signature of response to fulvestrant in advanced hormone receptor-positive breast cancer. *Clin. Cancer Res.* 22, 5755–5764.
- Koppen, A., Houtman, R., Pijnenburg, D., Jeninga, E.H., Ruijtenbeek, R., and Kalkhoven, E. (2009). Nuclear receptor-coregulator interaction profiling identifies TRIP3 as a novel peroxisome proliferator-activated receptor gamma cofactor. *Mol. Cell Proteomics* 8, 2212–2226.
- Kornberg, R.D. (2005). Mediator and the mechanism of transcriptional activation. *Trends Biochem. Sci.* 30, 235–239.
- Kwiatkowski, N., Zhang, T., Rahl, P.B., Abraham, B.J., Reddy, J., Ficarro, S.B., Dastur, A., Amzallag, A., Ramaswamy, S., Tesar, B., et al. (2014). Targeting transcription regulation in cancer with a covalent CDK7 inhibitor. *Nature* 511, 616–620.
- Langmead, B., Trapnell, C., Pop, M., and Salzberg, S.L. (2009). Ultrafast and memory-efficient alignment of short DNA sequences to the human genome. *Genome Biol.* 10, R25.
- Larochelle, S., Merrick, K.A., Terret, M.E., Wohlbold, L., Barboza, N.M., Zhang, C., Shokat, K.M., Jallepalli, P.V., and Fisher, R.P. (2007). Requirements for Cdk7 in the assembly of Cdk1/cyclin B and activation of Cdk2 revealed by chemical genetics in human cells. *Mol. Cell* 25, 839–850.
- Li, W., Koster, J., Xu, H., Chen, C.H., Xiao, T., Liu, J.S., Brown, M., and Liu, X.S. (2015). Quality control, modeling, and visualization of CRISPR screens with MAGeCK-VISPR. *Genome Biol.* 16, 281.
- Loven, J., Hoke, H.A., Lin, C.Y., Lau, A., Orlando, D.A., Vakoc, C.R., Bradner, J.E., Lee, T.I., and Young, R.A. (2013). Selective inhibition of tumor oncogenes by disruption of super-enhancers. *Cell* 153, 320–334.
- Meerbrey, K.L., Hu, G., Kessler, J.D., Roarty, K., Li, M.Z., Fang, J.E., Herschkowitz, J.I., Burrows, A.E., Ciccia, A., Sun, T., et al. (2011). The pINDUCER lentiviral toolkit for inducible RNA interference in vitro and in vivo. *Proc. Natl. Acad. Sci. USA* 108, 3665–3670.
- Merenbakh-Lamin, K., Ben-Baruch, N., Yeheskkel, A., Dvir, A., Soussan-Gutman, L., Jeselsohn, R., Yelensky, R., Brown, M., Miller, V.A., Sarid, D., et al. (2013). D538G mutation in estrogen receptor-alpha: a novel mechanism for acquired endocrine resistance in breast cancer. *Cancer Res.* 73, 6856–6864.
- Neph, S., Kuehn, M.S., Reynolds, A.P., Haugen, E., Thurman, R.E., Johnson, A.K., Rynes, E., Maurano, M.T., Vierstra, J., Thomas, S., et al. (2012). BEDOPS: high-performance genomic feature operations. *Bioinformatics* 28, 1919–1920.
- Nettles, K.W., Bruning, J.B., Gil, G., Nowak, J., Sharma, S.K., Hahm, J.B., Kulp, K., Hochberg, R.B., Zhou, H., Katzenellenbogen, J.A., et al. (2008). NFκB selectivity of estrogen receptor ligands revealed by comparative crystallographic analyses. *Nat. Chem. Biol.* 4, 241–247.
- Robinson, D.R., Wu, Y.M., Vats, P., Su, F., Lonigro, R.J., Cao, X., Kalyana-Sundaram, S., Wang, R., Ning, Y., Hodges, L., et al. (2013). Activating ESR1 mutations in hormone-resistant metastatic breast cancer. *Nat. Genet.* 45, 1446–1451.
- Rosell, M., Nevedomskaya, E., Stelloo, S., Nautiyal, J., Poliandri, A., Steel, J.H., Wessels, L.F., Carroll, J.S., Parker, M.G., and Zwart, W. (2014). Complex formation and function of estrogen receptor alpha in transcription requires RIP140. *Cancer Res.* 74, 5469–5479.
- Shalem, O., Sanjana, N.E., Hartenian, E., Shi, X., Scott, D.A., Mikkelsen, T.S., Heckl, D., Ebert, B.L., Root, D.E., Doench, J.G., and Zhang, F. (2014). Genome-scale CRISPR-Cas9 knockout screening in human cells. *Science* 343, 84–87.
- Spoerke, J.M., Gendreau, S., Walter, K., Qiu, J., Wilson, T.R., Savage, H., Aimi, J., Deryck, M.K., Chen, M., Chan, I.T., et al. (2016). Heterogeneity and clinical significance of ESR1 mutations in ER-positive metastatic breast cancer patients receiving fulvestrant. *Nat. Commun.* 7, 11579.
- Subramanian, A., Tamayo, P., Mootha, V.K., Mukherjee, S., Ebert, B.L., Gillette, M.A., Paulovich, A., Pomeroy, S.L., Golub, T.R., Lander, E.S., and Mesirov, J.P. (2005). Gene set enrichment analysis: a knowledge-based approach for interpreting genome-wide expression profiles. *Proc. Natl. Acad. Sci. USA* 102, 15545–15550.
- Toy, W., Shen, Y., Won, H., Green, B., Sakr, R.A., Will, M., Li, Z., Gala, K., Fanning, S., King, T.A., et al. (2013). ESR1 ligand-binding domain mutations in hormone-resistant breast cancer. *Nat. Genet.* 45, 1439–1445.
- Toy, W., Weir, H., Razavi, P., Lawson, M., Goepert, A.U., Mazzola, A.M., Smith, A., Wilson, J., Morrow, C., Wong, W.L., et al. (2017). Activating ESR1 mutations differentially affect the efficacy of ER antagonists. *Cancer Discov.* 7, 277–287.
- Trapnell, C., Williams, B.A., Pertea, G., Mortazavi, A., Kwan, G., van Baren, M.J., Salzberg, S.L., Wold, B.J., and Pachter, L. (2010). Transcript assembly and quantification by RNA-Seq reveals unannotated transcripts and isoform switching during cell differentiation. *Nat. Biotechnol.* 28, 511–515.
- Wang, Q., Li, W., Zhang, Y., Yuan, X., Xu, K., Yu, J., Chen, Z., Beroukhim, R., Wang, H., Lupien, M., et al. (2009). Androgen receptor regulates a distinct transcription program in androgen-independent prostate cancer. *Cell* 138, 245–256.
- Wang, L., Wang, S., and Li, W. (2012). RSeQC: quality control of RNA-seq experiments. *Bioinformatics* 28, 2184–2185.
- Wang, S., Sun, H., Ma, J., Zang, C., Wang, C., Wang, J., Tang, Q., Meyer, C.A., Zhang, Y., and Liu, X.S. (2013). Target analysis by integration of transcriptome and ChIP-seq data with BETA. *Nat. Protoc.* 8, 2502–2515.
- Whyte, W.A., Orlando, D.A., Hnisz, D., Abraham, B.J., Lin, C.Y., Kagey, M.H., Rahl, P.B., Lee, T.I., and Young, R.A. (2013). Master transcription factors and mediator establish super-enhancers at key cell identity genes. *Cell* 153, 307–319.
- Xu, H., Xiao, T., Chen, C.H., Li, W., Meyer, C.A., Wu, Q., Wu, D., Cong, L., Zhang, F., Liu, J.S., et al. (2015). Sequence determinants of improved CRISPR sgRNA design. *Genome Res.* 25, 1147–1157.
- Yi, P., Wang, Z., Feng, Q., Pintilie, G.D., Foulds, C.E., Lanz, R.B., Lutdkte, S.J., Schmid, M.F., Chiu, W., and O'Malley, B.W. (2015). Structure of a biologically active estrogen receptor-coactivator complex on DNA. *Mol. Cell* 57, 1047–1058.
- Zhang, Y., Liu, T., Meyer, C.A., Eeckhoute, J., Johnson, D.S., Bernstein, B.E., Nusbaum, C., Myers, R.M., Brown, M., Li, W., and Liu, X.S. (2008). Model-based analysis of ChIP-seq (MACS). *Genome Biol.* 9, R137.

STAR★METHODS**KEY RESOURCES TABLE**

REAGENT or RESOURCE	SOURCE	IDENTIFIER
Antibodies		
Rabbit polyclonal anti-ER α	Santa Cruz	SC-543;RRID:AB_631471
Rabbit polyclonal anti-TFAP2C	Santa Cruz	H-77;RRID:AB-2286995
Mouse monoclonal anti-CDK7	Cell signaling	2916;RRID:AB-2077142
Rabbit polyclonal anti-HA	Abcam	Ab9110;RRID:AB_307019
Rabbit polyclonal anti H3K27Ac	Diagenode	C15410196;RRID:AB_2637079
Goat polyclonal anti-FOXA1	Abcam	Ab5089;RRID: AB_304744
Biological Samples		
Breast cancer metastatic tumors	DFCI	
Patient derived xenografts	DFCI	
Chemical, Peptides and Recombinant Proteins		
Beta-Estradiol	Sigma Aldrich	E2758
Fulvestrant	Sigma Aldrich	I4409
4-hydroxy-tamoxifen	Sigma Aldrich	H7904
THZ1	DFCI	
Critical Commercial Assays		
ThruPLEX-FD Prep Kit	Rubicon	R40048
TruSeq RNA Sample Preparation Kit	Illumina	RS-122-2010
Deposited data		
Raw RNAseq and ChIPseq data	This paper	GSE94493 and GSE106552
Experimental Models: Cell lines		
Human: MCF7	ATCC	HTB-22
Human: T47D	ATCC	HTB-133
Experimental Models: Organisms/strains		
<i>NOD-SCID-IL2Rγc^{-/-}</i> mice	Jackson Lab	005557
Oligonucleotides		
Mutagenesis primers	This manuscript	
Y537N: Forward, 5'- AACGTGGTGCCCTCAATGACCTGCTGGAGA T -3'		
Y537N: Reverse, 5'- ATCTCCAGCAGCAGGTCAATTGAGGGGCACCAAGTT -3'		
Y537S: Forward, 5'- AACGTGGTGCCCTCTGACCTGCTGGAGAT -3'		
Y537S:Reverse, 5'- ATCTCCAGCAGCAGGTCAAGAGAGGGGCACCAAGTT -3'		
D538G: Forward, 5'- AACGTGGTGCCCTCTATGGCCTGCTGGAGAT -3'		
D538G:Reverse, 5'-ATCTCCAGCAGCAGGCCATAGAGGGGCACCAAGTT -3'		
TALEN sequences	This manuscript	
XTN1: 5'TCCCAGCTCCATCTAA AGTGGGTCTTAAACAGGAAGAAAGAAAGATTGCTA 3'		
XTN2: 5'TCAGCTTCCCAGCTCC ATCCTAAAGTGGGTCTTAAACAGGAAGAAAGAA3 '		
TFAP2C gRNAs:		
gRNA1:F: 5'CACCGCGAATTCTAGTAAACCAG3'		
gRNA1 R: 5' AAACCTGGTTACTAGGAAATTGCG3'		
gRNA2:F:5'CACCGCAGCTCCTCTGACAGGGG3'		

(Continued on next page)

Continued

REAGENT or RESOURCE	SOURCE	IDENTIFIER
gRNA2 R: 5' AAACCCCTGTCAGAAGGAGCTGC3'	This manuscript	
CDK7 gRNAs:		
gRNA1:F:5'CACCGGAAGCTGGACTTCCTGGGG3'		
gRNA1:R:5'AAACCCCCAAGGAAGTCCAGCTTCC3'		
gRNA2:F:5'CACCGATCTCTGGCCTGTAAACGG3'		
gRNA2:R:5'AAACCCGTTACAAGGCCAGAGATC3'		
gRNA3:F:5'CACCGATGTGTATAAGCTCTATTG3'		
gRNA3:R:5'AAACCAATAGAGCTTACACATC3'	This manuscript	
FOXA1 gRNAs:		
gRNA1: F:5' CACTACTACGCAGACACGCAGG3'		
gRNA1: R: 5'AAA ATGATGCGTCTGTGCGTCC3'		
gRNA2: F 5'CACGACATGTTGAAGGACGCCG3'		
gRNA2: R: 5'AAACTGTACAACCTCCTGCGGC3'		
Recombinant DNA		
pInducer	This manuscript	
LentiCRISPR V2		
Software and Algorithms		
MACS 2.0	This manuscript	
Bamliquidator		
Binding and Expression Target Analysis (BETA)		
MEME	Meerbrey, et al	Elledge lab
ROSE	Addgene	49535
	Feng et al	
		https://github.com/BradnerLab/pipeline/wiki/bamliquidator
		Cistrome. org
		https://bitbucket.org/young_computation/rose.git

CONTACT FOR REAGENT AND RESOURCE SHARING

Further information and requests for resources and reagents should be directed and will be fulfilled by the Lead Contact Myles Brown (myles_brown@dfci.harvard.edu).

EXPERIMENTAL MODEL AND SUBJECT DETAILS**Cell Lines**

MCF7 and T47D cells were purchased from ATCC. All the cells were authenticated and regularly tested for mycoplasma contamination. The MCF7 cells were maintained in DMEM and T47D cells in RPMI supplemented with 10% heat-inactivated fetal bovine serum (FBS) and 1% penicillin/streptomycin (P/S). For hormone-depleted (HD) conditions, cells were kept in phenol-red free medium supplemented with 10% heat-inactivated charcoal-stripped (CS)-FBS and 1% PS. All cells were incubated at 37°C in 5% CO₂.

In Vivo Animal Studies

All mice were maintained in accordance with local guidelines and therapeutic interventions approved by the Animal Care and Use Committees of Dana-Farber Cancer Institute. For the PDX studies, patient consent for tumor implantation in nude mice was obtained under protocols approved by the IRB of the Dana-Farber/Harvard Cancer Center. ER⁺ metastatic tumor samples were implanted into the cleared fourth mammary fat pads of *NOD-SCID-IL2Rγc^{-/-}* mice (Jackson Laboratories) treated with an E2 pellet. Mice were all females and five weeks old. Similarly, for the orthotopic xenografts derived from cell lines, *NOD-SCID-IL2Rγc^{-/-}* mice female 5 weeks old mice (Jackson Laboratories) were used.

Human Tissue Studies

All patients provided written informed consent for research metastatic biopsies and genomic profiling of tumor RNA, as approved by the Dana-Farber/Harvard Cancer Center Institutional Review Board (DF/HCC Protocol 05-246). Core biopsies were obtained from patients with metastatic ER+ breast cancer. After the core biopsy, samples were immediately snap frozen in OCT and stored in -80C freezer.

METHOD DETAILS

Generation of DOX-Inducible WT and Mutant ER Cells

For the DOX-inducible ER mutant and WT-ER cells, ER-HA tag cDNA (GeneCopoeia) was transferred to the pInducer 20 destination vector (Meerbrey et al., 2011) using the Gateway system (Invitrogen). Lentivirus was produced in 293T cells to infect cells in media containing polybrene (8 μ g/mL). Cells were selected after the infection with G418. The GeneArt Site-Directed mutagenesis system (Life Technologies) was used to generate Y537N, Y537S and D538G mutations within the ER ligand-binding domain. The following mutagenesis primers were used:

1. Y537N: Forward, 5'- AACGTGGTGCCCTCAATGACCTGCTGCTGGAGAT -3' Reverse, 5'- ATCTCCAGCAGCAGGTCATTGAG GGGCACACCACGTT -3'
2. Y537S: Forward, 5'- AACGTGGTGCCCTCTGACCTGCTGCTGGAGAT -3'
Reverse, 5'- ATCTCCAGCAGGGTCAGAGAGGGGCACCACGTT -3'
3. D538G: Forward, 5'- AACGTGGTGCCCTTATGGCCTGCTGGAGAT -3'
Reverse, 5'- ATCTCCAGCAGGGCCATAGAGGGGCACCACGTT -3'.

Sanger sequencing and RNA-sequencing confirmed the desired mutations.

Generation of Transcription Activator Like Nucleases (TALEN) Mediated Mutant Cells

The *ESR1* Y537S and D538G knock-in mutant cells were generated in MCF7 cells. The TALENs were designed to target intron 7 and the TALEN recognition sequences were:

XTN1: (bold=cut region, non-bold=TAL binding sites)
5'TCCCAGCTCCCATCCTAAAGTGGTCTTAAACAGGAAGAAAGAAAGATTGCTA3'
 XTN2: (bold=cut region, non-bold=TAL binding sites)
5'TCAGCTTCCCAGCTCCATCCTAAAGTGGTCTTAAACAGGAAGAAAGAA3'

The sequences were synthesized and cloned into the SQT281 vector (Transposagen) that includes a Fok1 nuclease. For the homologous recombination we used a donor vector that contained the targeting constructs of *piggyBac* transposon and the a puromycin-thymidine kinase (TK) selection cassette flanked by 500 bp of *ESR1* genomic sequence with the coding changes (TAT>TCT for Y537S and GAC>GGC for G538G) in the 3' end matching the exon 8 coding region. The MCF7 cells were transiently transfected with the TALEN vector and donor vector using Lipofectamine 2000 (Invitrogen). After puromycin selection, clones with the desired mutation were identified by Sanger sequencing and transiently transfected with transposase expression plasmids (Transposagen) for removal of the selection cassettes followed by gancyclovir treatment for negative selection to enable a "foot-print free" knock-in cell lines. We confirmed the mutations by Sanger sequencing and RNA-sequencing.

Proliferation Assays

The breast cancer cells were plated in 24 well plates. At indicated time points, the cells were counted using the Celigo image Cytometer (Nexcelom). Hoescht was used for nuclear staining and propidium iodide was used for staining dead cells. For the dose response studies and determination of the IC50's 4-hydroxytamoxifen (Sigma-Aldrich, catalog # H7904), fulvestrant (Sigma catalog #I4409) and THZ1 (Nathanael Gray's lab, Dana Farber Cancer Institute) were used.

Western-Blotting

For Western blot analysis, cells were lysed in 50mM Tris-HCl pH 7.5, 150mM NaCl, 1mM EDTA, 1mM EGTA, 0.5% NP-40, 1% Triton X-100 supplemented with protease inhibitors and subjected to SDS-PAGE. Antibodies used were: ER α (sc-543, Santa Cruz), TFAP2C (Santa Cruz), CDK7 (Cell Signaling, 2916), ER-S118 (Cell Signaling, 2511), Beta-Actin (Sigma), GAPDH (Santa Cruz), HA (Ab9110, Abcam).

Chromatin Immunoprecipitation (ChIP)-Sequencing

ChIP experiments were conducted as described previously (Wang et al., 2009) and were done in triplicates. Chromatin from approximately 1×10^7 fixed cells was sonicated to a size range of 200-300 bp. Solubilized chromatin was subjected to immunoprecipitation with the ER antibody, Ab10 (Lab Vision corporation) and SC-543 (Santa cruz), HA antibody (Ab9110, Abcam), H3K27Ac antibody (C15410196, Diagenode) or FOXA1 (ab5089, Abcam) bound to protein A and protein G beads (Life Technologies). A fraction of the sample was not exposed to antibody to be used as control (input). The samples were reversed crosslinked, treated with proteinase K, and DNA was extracted. DNA sequencing libraries were prepared using the ThruPLEX-FD Prep Kit (Rubicon Genomics). Libraries were sequenced using 50 bp reads on the Illumina Nextseq500 at the Dana-Farber Cancer Institute.

RNA Sequencing

Total RNA was isolated using an RNeasy Mini Kit (Qiagen). For all cell line studies samples were done in triplicates. RNA-seq libraries were made using the TruSeq RNA Sample Preparation Kit (Illumina) adapted for use on the Sciclone (Perkin-Elmer) liquid handler. Samples were sequenced on an Illumina Nextseq500.

Co-Regulator Interaction Profiling

This method has been described previously (Koppen et al., 2009). Cell lysates of each clone were prepared and ER α was quantified by ELISA (Active Motif, USA) to enable equimolar input. An array with a set of immobilized peptides representing coregulator-derived NR-binding motifs is incubated with a reaction mixture of crude lysate, vehicle (2% DMSO) with or without 1 μ M 17- β -estradiol (E2) and anti-HIS-Alexa488 (Qiagen, USA). Incubation was performed for 40 minutes at 20°C, followed by removal of unbound receptor by washing and generation of a tiff image of each array using a PamStation96 (PamGene International). Image processing and quantification of ER α binding to each peptide on the array was performed by Bionavigator software (PamGene International). The list of protein peptides evaluated detailed in Table S4.

CRISPR Knock-Out Library Screen

To design an efficient genome-wide CRISPR-Cas9 library for screening, we first scanned human genome to select gRNAs with an “NGG” PAM sequence motif adjacent to its 3' end. Then we predicted efficiency score of each gRNA based on our Least Absolute Shrinkage and Selection Operator (LASSO) model (Xu et al., 2015). We further selected the putative 19bp sgRNA targets that are within the exons of the genes selected for screening, have the best predicted efficiency score and have no mutation relative to the reference genome in any cancer cell line (COSMIC). To minimize off-target effects, we aligned the 19bp sequences of the putative targets against all exons in the genome. The gRNAs with fewer than 2 mismatches in the secondary match outside the target gene were removed. In the library, we also included two types of negative controls: i) non-specific sgRNAs that are not mappable to human genome; ii) sgRNAs targeting the AAVS1 integration locus where insertion or deletion does not affect cell function. Taken together, the lentivirus library consisted of 183128 gRNAs for 18313 protein-coding genes, 730 gRNAs for ribosomes, 385 gRNAs for non-targeting controls, and 136 gRNAs for AAVS1 controls. The sgRNA library synthesized at CustomArray and amplified by PCR as previously described (Shalem et al., 2014). The PCR products were subsequently ligated into lentiCRISPR V2 plasmid, followed by transformation to competent cells for amplification according to the online protocol GeCKO library Amplification Protocol from Addgene. After plasmid library was amplified, we isolated the plasmid and constructed a sequencing library for Miseq to ensure library diversity. The DOX-inducible cells were infected at a low MOI (0.2) to ensure that most cells receive only one viral construct with high probability. Large-scale infection of 2×10^8 cells was carried. After five days of puromycin selection, the surviving cells were divided into day 0 control cells and cells cultured for five weeks before genomic DNA extraction and library preparation. Each library was sequenced at 25 million reads to achieve ~300X average coverage over the CRISPR library. The 0 day sample library of each screen served as controls to identify positively or negatively selected genes or pathways.

Generation of Single CRISPR/Cas9 Knock-Out Cells

Construction of lenti-CRISPR/Cas9 vectors targeting transcriptional CDK was performed following the protocol associated with the backbone vector (49535, Addgene). The following sgRNA sequences were used:

TFAP2C Guides:

gRNA1:F:5'CACCGCGAAGCTGGACTTCCCTGGGG3'
gRNA1 R: 5' AACCTGGTTACTAGGAAATCG3'
gRNA2:F:5'CACCGCAGCTCCTCTGACAGGGG3'
gRNA2 R: 5' AAACCCCCTGTCAGAAGGAGCTGC 3'

CDK7 Guides:

gRNA1:F:5'CACCGGAAGCTGGACTTCCCTGGGG3'
gRNA1 R:5'AAACCCCCAAGGAAGTCAGCTTC3'
gRNA2:F:5'CACCGATCTCTGGCCTTGAAACGG3'
gRNA2 R:5'AAACCGTTACAAGGCCAGAGATC3'
gRNA3:F:5'CACCGATGTATAAGCTTATTG3' rv: gRNA3 R:5'AAACCAATAGAGCTTACACATC3'

FOXA1 Guides:

gRNA1: F:5' CACTACTACGCAGACACGCAGG3'
gRNA1: R: 5'AAA ATGATGGTCTGTGCGTCC3'
gRNA2: F 5'CACGACATGTTGAAGGACGCCG3'
gRNA2: R: 5'AAACTGTACAACCTCCTGCGGC3'

Drug Synergy Studies

Cells were plated in 96 wells and treated with vehicle and 2 fold serial dilutions for 6 doses of THZ1(2.5, 5, 10, 20, 40 and 80 nM) and fulvestrant(1.2, 2.5, 5, 10, 20 and 40 nM) in a matrix format to include 49 different dose combinations. Viable cells were counted on day 5 with the Celigo image Cytometer (Nexcelom).

QUANTIFICATION AND STATISTICAL ANALYSIS

Statistical analyses for cell proliferation studies were performed using two sided Student's t-tests, and p values less than 0.05 were considered statistically significant. Error bars represent the \pm SEM. Cell line experiments testing cell proliferation were all performed in triplicates.

RNA Sequencing Analysis

Alignment to the hg19 human genome was done using STAR v2.5.1([Dobin et al., 2013](#)) followed by Transcript assembly using cufflinks v2.2.1([Trapnell et al., 2010](#)) and quality control steps were done using STAR v2.5.1 and RseQC v2.6.2([Wang et al., 2012](#)). We assessed each sample on metrics of mappable reads, percentage of rRNA reads, gene body coverage, and junction saturation and insert_size for paired end, to determine samples that were of adequate quality. Differential Expression Analysis was done using DEseq2 v1.1([Wang et al., 2012](#)). GSEA analysis was performed using the Broad GSEA Application ([Subramanian et al., 2005](#))

ChIP Sequencing Analysis

ChIP-seq reads were aligned to the hg19 genome assembly using Bowtie([Langmead et al., 2009](#)) and ChIP-seq peaks were called using MACS 2.0 ([Feng et al., 2012; Zhang et al., 2008](#)). For differential binding analysis, bedfiles were merged using bedops ([Neph et al., 2012](#)) and then Bamliquidator (<https://github.com/BradnerLab/pipeline/wiki/bamliquidator>) was used to assign a binding intensity score to each region of the merged bed file. Differential binding was determined by filtering out insignificantly binding peaks (Bamliquidator score < 0.1) and then determining log2FC values between samples for each region using a log2 FC >1 or <-1. For the Binding and Expression Target Analysis (BETA) correlative analysis with RNA-seq differential expression the peaks were defined into region bed files including upbound peaks (log2FC > 1), downbound peaks (log2FC < -1), and nodiff peaks (log2FC < 1 and >-1). Each of these bed files was paired with the associated differential gene expression including only the differential genes with an adjusted p-value of <0.1. We took the outputted BETA bed files, added up the BETA scores for each gene and normalized each BETA score by dividing by the original number of peaks entered into BETA. Then for each of the three files, we binned the genes by log2FC into bins of 100, and plotted out the average log2FC of gene expression, and the average normalized BETA score for each bin.

The motif analysis was done using the MEME suite tool AME (Analysis of Motif Enrichment)([Bailey et al., 2015](#)).

To identify super-enhancers, we employed the ROSE algorithm to rank the enhancers that were identified using MACS in which peaks from H3K27ac ChIP within 12.5 kb of one another were stitched together ([Loven et al., 2013; Whyte et al., 2013](#)). These stitched enhancers were ranked by their difference in H3K27ac signal versus input signal.

A threshold separating super-enhancers from typical enhancers was identified by finding the point at which the line Y=X was tangent to the curve formed by plotting the stitched enhancer rank versus H3K27ac signal subtracting the input signal.

CRISPR/CAS9 Library Screen Analysis

The CRISPR/Cas9 screening data was processed and analyzed using the MAGeCK and MAGeCK-VISPR algorithms previously published ([Li et al., 2015](#)). MAGeCK-VISPR uses a metric, “ β score”, to measure gene selections. The definition of β score is similar to the term of ‘log FC’ in differential expression analysis, and $\beta>0$ (or <0) means the corresponding gene is positively (or negatively) selected, respectively. We considered a β score of >0.5 or <-0.5 as significant. MAGeCK-VISPR models the gRNA read counts as a negative binomial variable, whose mean value is determined by the sequencing depth of the sample, the efficiency of the gRNA, and a linear combination of β scores of the genes. MAGeCK-VISPR then builds a maximum likelihood (MLE) model to model all gRNA read counts of all samples, and iteratively estimate the gRNA efficiency and gene β scores using the Expectation-Maximization algorithm.

Drug Synergy Analysis

Drug synergy was calculated based on the Bliss independence model using the SynergyFinder R package ([Ianevski et al., 2017](#)).

DATA AVAILABILITY

The RNA-seq and ChIP-seq data have been deposited in the Gene Expression Omnibus database. The accession numbers for the sequencing data reported in this paper are GSE94493 and GSE106552.